THIS MANUSCRIPT HAS BEEN SUBMITTED TO THE JOURNAL OF GLACIOLOGY AND HAS NOT BEEN PEER-REVIEWED.

Ice Surface Change Drives Subglacial Hydrologic Reorganization and Interior Speedup in Northwest Greenland

Journal:	*Journal of Glaciology*
Manuscript ID	JOG-2026-0033.R1
Manuscript Type:	Article
Date Submitted by the Author:	n/a
Complete List of Authors:	Sommers, Aleah; Dartmouth College, Thayer School of Engineering Stubblefield, Aaron; University of Maryland; NASA Goddard Space Flight Center Andrews, Lauren; NASA Goddard Space Flight Center, Cryospheric Sciences Labratory Meyer, Colin; Dartmouth College, Thayer School of Engineering Smith, Benjamin; University of Washington,
Keywords:	Subglacial processes, Laser altimetry, Ice-sheet modelling, Glacier hydrology, Arctic glaciology
Abstract:	Changes in ice surface elevation and slope influence subglacial water pressure and sliding velocity. Leveraging changes in elevation observed by the Ice, Cloud, and land-Elevation satellite (ICESat) and ICESat-2 missions, we use coupled subglacial hydrology--ice dynamics modeling applied to a section of the northwest Greenland Ice Sheet to explore i) how decadal scale changes in ice surface elevation influence changes in winter background subglacial hydrology and corresponding ice velocity, and ii) how much seasonal response is attributable to geometry versus environmental forcing. Our simulations suggest complex reorganization of the subglacial hydrologic system between 2004 and 2020, resulting from changes in surface elevation, driving redistribution of freshwater flux, an overall acceleration trend in the interior, and an increase in background basal melt. Without changing hydrological conditions, geometry changes

	alone lead to greater interior acceleration, suggesting that changes in the subglacial system help to mitigate this speedup. We also find that the winter background state of the subglacial system modulates the seasonal response. This work demonstrates feedbacks that influence mass loss from the Greenland Ice Sheet as surface elevation evolves, highlighting the subtleties involved in accounting for changes in effective pressure, ice velocity, and basal melt due to changes in subglacial hydrology.

Journal of Glaciology, Vol. ?, No. ?, 2026 1

Ice Surface Change Drives Subglacial Hydrologic Reorganization and Interior Speedup in Northwest Greenland

Aleah N. SOMMERS,[1] Aaron STUBBLEFIELD,[2,3] Lauren ANDREWS,[3] Colin R. MEYER,[1] Benjamin E. SMITH[4]

[1] *Thayer School of Engineering, Dartmouth College, Hanover, NH, USA*

[2] *University of Maryland, College Park, MD, USA*

[3] *NASA Goddard Space Flight Center, Greenbelt, MD, USA*

[4] *Applied Physics Laboratory, University of Washington, Seattle, WA, USA*

Correspondence: Aleah Sommers <aleah.n.sommers@dartmouth.edu>

ABSTRACT. Changes in ice surface elevation and slope influence subglacial water pressure and sliding velocity. Leveraging changes in elevation observed by the Ice, Cloud, and land-Elevation satellite (ICESat) and ICESat-2 missions, we use coupled subglacial hydrology–ice dynamics modeling applied to a section of the northwest Greenland Ice Sheet to explore i) how decadal scale changes in ice surface elevation influence changes in winter background subglacial hydrology and corresponding ice velocity, and ii) how much seasonal response is attributable to geometry versus environmental forcing. Our simulations suggest complex reorganization of the subglacial hydrologic system between 2004 and 2020, resulting from changes in surface elevation, driving redistribution of freshwater flux, an overall acceleration trend in the interior, and an increase in background basal melt. Without changing hydrological conditions, geometry changes alone lead to greater interior acceleration, suggesting that changes in the subglacial system help to mitigate this speedup. We also find that the winter background state of the subglacial system modulates the seasonal response. This work demonstrates feedbacks that influence mass loss from the Greenland Ice Sheet as surface elevation evolves, highlight-

ing the subtleties involved in accounting for changes in effective pressure, ice velocity, and basal melt due to changes in subglacial hydrology.

INTRODUCTION

The Greenland Ice Sheet is a prominent frozen reservoir of freshwater on Earth. In recent decades, it has had a negative mass balance, losing more ice through melt, runoff, and iceberg calving than it gains each year through snow accumulation that gradually compacts into ice (Mouginot and others, 2019; Mankoff and others, 2020). Although widespread satellite observations in recent years have improved the monitoring of overall mass loss of the Greenland Ice Sheet (Shepherd and others, 2012; Hanna and others, 2013; Mouginot and others, 2019; Smith and others, 2019), gaps remain in scientific understanding of the physical processes governing dynamics of the ice sheet and how these will impact mass loss in the future. A particular source of uncertainty in future sea level projections associated with ice mass loss is the role of subglacial hydrology, or liquid water at the interface between the ice and the underlying bed material. The subglacial environment is difficult to access for direct observations, but numerical models can provide insights into basal processes by simulating the relevant physical processes of water and ice flow, melt, and sliding.

Subglacial hydrology affects the velocity of glaciers by modulating how easily the ice slides over its bed. Glacier sliding parameterizations (or "sliding laws") are generally formulated in terms of basal stress, calculated as a function of ice sliding velocity and effective pressure, which is defined as the difference between ice overburden pressure and water pressure at the bed (Budd and others, 1979; Schoof, 2005). The specific relationship and exponents vary between different sliding laws, but sliding velocity and effective pressure typically have a nonlinear relationship.

Water below glaciers flows according to pressure gradients, which are partly determined by geometric properties of the glacier, such as surface slope, ice thickness, and bed slope, and partly by fluid flow dynamics. Pressure evolves dynamically through space and time with evolving glacier geometry and hydraulic processes. Water moves from high to low pressure, meaning that in some cases water can flow uphill relative to the bed or surface topography. Although bed topography beneath the ice is difficult to accurately constrain, ice surface elevation has been relatively well observed since 2003 with NASA's Ice, Cloud and land-Elevation satellite (ICESat) and follow-up Operation IceBridge (MacGregor and others, 2021) and ICESat-2 laser altimetry missions, by which the travel time of laser pulses is used to measure the elevation of Earth's surface (Schutz and others, 2005; Abdalati and others, 2010; Markus and others, 2017). Changes in ice surface elevation and surface slope cause changes in the hydraulic pressure gradient at the bed.

Liquid water beneath glaciers is derived from melting at the base of the ice as well as seasonal surface melting that drains through the ice. During the winter months, the subglacial system receives water primarily from basal melt and is in a relatively stable background state. During the summer months, a significant fraction of the water that melts on the surface of the ice sheet drains to the bed via moulins and crevasses (Meierbachtol and others, 2013; Andrews and others, 2014; Smith and others, 2015). At higher elevations, a portion of surface melt percolates into porous firn and refreezes instead of running off (Meyer and Hewitt, 2017; Rennermalm and others, 2022). Intuitively, one might expect that more meltwater being produced on the ice sheet would lead to more water at the bed, and a corresponding increase in water pressure and acceleration. However, this is not necessarily the case – as has been observed through field observations and represented in numerical models (Schoof, 2010; Flowers, 2015) – with sufficient meltwater inputs to the bed, the drainage system will transition to form an efficient system of channelized pathways. These efficient conduits decrease water pressure and consequently pull water from the surrounding bed, increasing friction and yielding a deceleration even with increasing melt (Sundal and others, 2011). This negative feedback complicates predicting future development of Greenland glacier seasonal velocities, and numerous scientific studies have attempted to understand when and where such channelized drainage is likely to develop (Banwell and others, 2016; Cowton and others, 2016; Simkins and others, 2021; Rada Giacaman and Schoof, 2023; Warburton and others, 2024).

In this study, we are motivated by questions that address the impact of the background state and seasonal evolution of the subglacial system: 1) How do decadal scale changes in surface elevation influence changes in winter background state subglacial hydrology and corresponding ice dynamics of the Greenland Ice Sheet? 2) How much is seasonal velocity attributable to glacier geometry compared to environmental forcing? Leveraging ice surface elevation derived from ICESat and ICESat-2 observations, we use a coupled subglacial hydrology–ice dynamics model to simulate changes in effective pressure and ice velocity over the period 2004 to 2020.

In the following sections, we describe our methods, including how we generate our high-resolution DEMs, the models and data we use, and our experimental approach. We then present simulation results and discuss implications of our findings.

METHODS

DEM generation

We generate high-resolution DEMs of the Greenland Ice-Sheet surface based on a combination of ICESat and ICESat-2 satellite laser altimetry, Operation IceBridge airborne laser-altimetry data, and ArcticDEM digital elevation models. We combine these using a surface-fitting algorithm adapted from the algorithm developed for the ICESat-2 ATL14 and ATL15 gridded height and height-change data products, with additional processing steps added to help correct for potential artifacts in the other datasets. The ATL14/15 algorithm (Smith and others, 2026, 2025) approximates ice-sheet elevations as the sum of a fine-resolution reference DEM and a set of coarser-resolution elevation-change surfaces. For example, the ICESat-2 project generates a 100-m DEM (ATL14) and a set of elevation-change surfaces with 1 km horizontal and 0.25 yr temporal resolution. The algorithm works by minimizing a functional that depends on the roughness of the DEM, the roughness of the elevation-change rate described by the elevation-change surfaces, and the uncertainty-scaled misfit between the estimated elevation (equal to the sum of the DEM and the elevation-change surfaces) and the ICESat-2 data points. The combined ATL14 and ATL15 data products give well constrained estimates of surface height during the ICESat-2 mission (2019-2025) along reference ground tracks that ICESat-2 has measured repeatedly, but the accuracy of the surface-height estimates declines in the gaps between these tracks (Smith and others, 2026). We use a modified version of this algorithm with an extended set of input data products to generate a set of high-resolution DEMs spanning 2004-2020.

Our DEM generation is carried out in two stages. In the first stage, we apply the surface-fitting algorithm to a combination of ICESat-2 and ArcticDEM data to generate a high-resolution (50 m) DEM referenced to decimal year 2020.5. In the second stage, we subtract this DEM from a multi-decadal time series of ICESat and IceBridge laser-altimetry data to produce a set of elevation-difference measurements spanning 2004-2020. We then apply the surface-fitting algorithm to these difference measurements to produce a time series of gridded elevation differences with 500 m horizontal and 1 yr temporal node spacing. See the Supplemental Information for more details.

Model description

To simulate subglacial hydrology, we use the Subglacial Hydrology And Kinetic, Transient Interactions model (SHAKTI; Sommers and others (2018)) coupled with ice dynamics in the Ice-sheet and Sea-level

System Model (ISSM; Larour and others (2012)). SHAKTI is a physics-based model that calculates evolving hydraulic head, effective pressure, subglacial gap height, water flux, and basal melt. The model internally calculates spatiotemporally variable hydraulic transmissivity, allowing for turbulent, laminar, and transitional flow regimes to develop, and flexible drainage geometries to emerge that represent a continuum from inefficient/distributed drainage, to efficient/channelized drainage. ISSM is a state-of-the-art glacier ice flow model that uses finite element methods on adaptable meshes to simulate a variety of processes that impact ice dynamics. SHAKTI is built into ISSM as a module to facilitate coupling between subglacial hydrology and ice velocity, which occurs through the friction parameterization, or sliding law, in which basal stress depends on both effective pressure (calculated by SHAKTI) and ice sliding velocity (calculated by the stress balance in ISSM). We use the same form of the SHAKTI equations as in Sommers and others (2024). The simulations presented in this paper use the Budd-type sliding law (Budd and others, 1979) and the Shallow Shelf Approximation (SSA) (MacAyeal, 1989) for ice flow. See Table S1 for a list of parameter values.

In the Budd friction parameterization, basal stress τ_b is calculated as:

$$\tau_b = C^2 N u_b, \tag{1}$$

where C is a spatially variable friction coefficient, N is effective pressure, and u_b is ice sliding velocity (which is equivalent to the depth-integrated velocity in the SSA ice flow approximation used here).

In an effort to keep the model relatively simple while including hydrology and velocity coupling, we assume an average bulk ice temperature of -10 degrees C for the entire domain, with ice rheology (Glen's flow law coefficient) based on that temperature. This same rheology applies to SHAKTI and appears in the creep closure of the subglacial system, which depends on the flow law parameter. The basal melt rate calculation implicitly assumes that water and ice directly at the bed are both at the pressure melting point. No-flux Neumann boundary conditions are applied along the domain boundaries, and a Dirichlet boundary condition setting hydraulic head to zero is applied to ice-free nodes and where ice thickness is less than 10 m. Assuming that fjord water is well mixed with fresh water near the terminus of marine-terminating glaciers, this sets the subglacial discharge water pressure equal to the hydrostatic pressure of the overlying water depth in the fjord at the terminus. We begin with an initial subglacial gap height of 0.01 m and use a time step of 1 hour.

Our model domain is a region in Northwest Greenland (Fig. 2a), selected as a focus area because of its significant change in surface elevation and numerous fjords with outlet glaciers. The finite element mesh consists of 129,273 triangular elements, using adapted resolution based on observed surface velocity, with element edge lengths ranging from 100 m to 20 km. We use ice thickness and bed elevation estimates from BedMachine v5 (Morlighem and others, 2021) to set the ice geometry for 2004. Bed elevation is held consistent for all other years, while the ice thickness changes corresponding to changes in ice surface elevation. After prescribing the 2004 ice geometry for our domain, we perform an inversion to infer the pattern of the spatially variable friction coefficient C used in Eq. 1, assuming in the inversion perfect connectivity to the ocean (i.e. hydraulic head equals zero and effective pressure is purely a function of ice geometry). This is similar to the iterative inversion initialization process described in Sommers and others (2024) but with only one inversion. In standard practice ice sheet modeling, the friction coefficient is typically used to represent the lumped influence of variable conditions at the bed necessary to reproduce observed velocity patterns, including variations in effective pressure. Because we explicitly account for spatial and temporal variations in effective pressure in our coupled hydrology simulations, here the friction coefficient primarily represents variations in bed material properties that influence basal friction and presumably remains relatively unchanged over the decadal time scales considered here. We hold this friction coefficient distribution consistent in all our simulations, and the basal stress obviously evolves with changes in effective pressure. This is in contrast to the transient calibration approach of Badgeley and others (2025), for example, in which sequential inversions are performed to infer changes in friction coefficient, assuming a static effective pressure distribution.

Winter background hydrology and velocity

We run coupled SHAKTI-ISSM spin-up simulations for one year to generate the winter "background state" hydrology and velocity conditions for snapshots at 2004, 2008, 2012, 2016, and 2020, with ice geometry based on the derived DEM for each year described above. Ice geometry remains unchanged during each simulation, with surface elevation set by the DEM for each year. Ice thickness and terminus positions do not transiently evolve during a simulation. In these winter simulations, we assume that all meltwater present in the subglacial system is produced by basal melt through a combination of geothermal flux, frictional heat from sliding, and turbulent dissipation. The winter background sets the initial conditions for the melt season in Greenland, with drainage structures sustained below the ice even in the absence of large surface meltwater inputs. Far from being stagnant, active subglacial hydrological systems persist through the winter, supplied by basal melt (Sommers and others, 2023).

Seasonal simulations

Beginning from our winter background state simulations for 2004 and 2020, we run transient seasonal simulations using ice sheet surface runoff derived from the MERRA-2 climate reanalysis (Gelaro and others, 2017) to prescribe the magnitude, timing, and distribution of meltwater inputs to the bed. We direct all surface runoff immediately to the bed at the location where the water is produced, neglecting the nuances of routing, refreezing, or storage in the supraglacial and englacial drainage systems. In order to uniquely assess the role of surface geometry in determining hydrological and ice flow under comparable environmental forcing, we force these transient simulations on 2004 and 2020 geometries using the same seasonal runoff data from the mean climatology over the period 2003-2022.

Ice velocity comparison to observations

In order to assess the impact of surface elevation change on ice velocity patterns relative to observations, we compare the modeled winter background states to winter time SAR derived ice velocities (Joughin and others, 2010, 2015, 2018; Joughin, 2023). To complete this analysis, we use observations dated from 2000 to 2020; 2000 is used because the next image is from 2005/2006. Table S2 presents a list of the specific images used. Velocity images span variable ranges, but do not include the summer melt season (June, July and August). We then calculate the linear velocity trend of each pixel. Using the linear trend, we determine the expected velocity at the model time steps of 2004.5 and 2020.5. We perform the same analysis for the winter background model outputs after regridding the model outputs to the observational grid of 500 m x 500 m. This processing permits us to directly compare the observations and model outputs while minimizing the impact of interannual variability.

MODEL RESULTS

Figure 1 presents ice surface velocity, subglacial water flux, and effective pressure modeled using 2004 and 2020 surface elevations. Modeled velocity, water flux, and effective pressure all vary spatially, and overall display the same large-scale structure in both years. The differences between the two, however, reveal notable changes attributable to changes in surface elevation. These changes are discussed next.

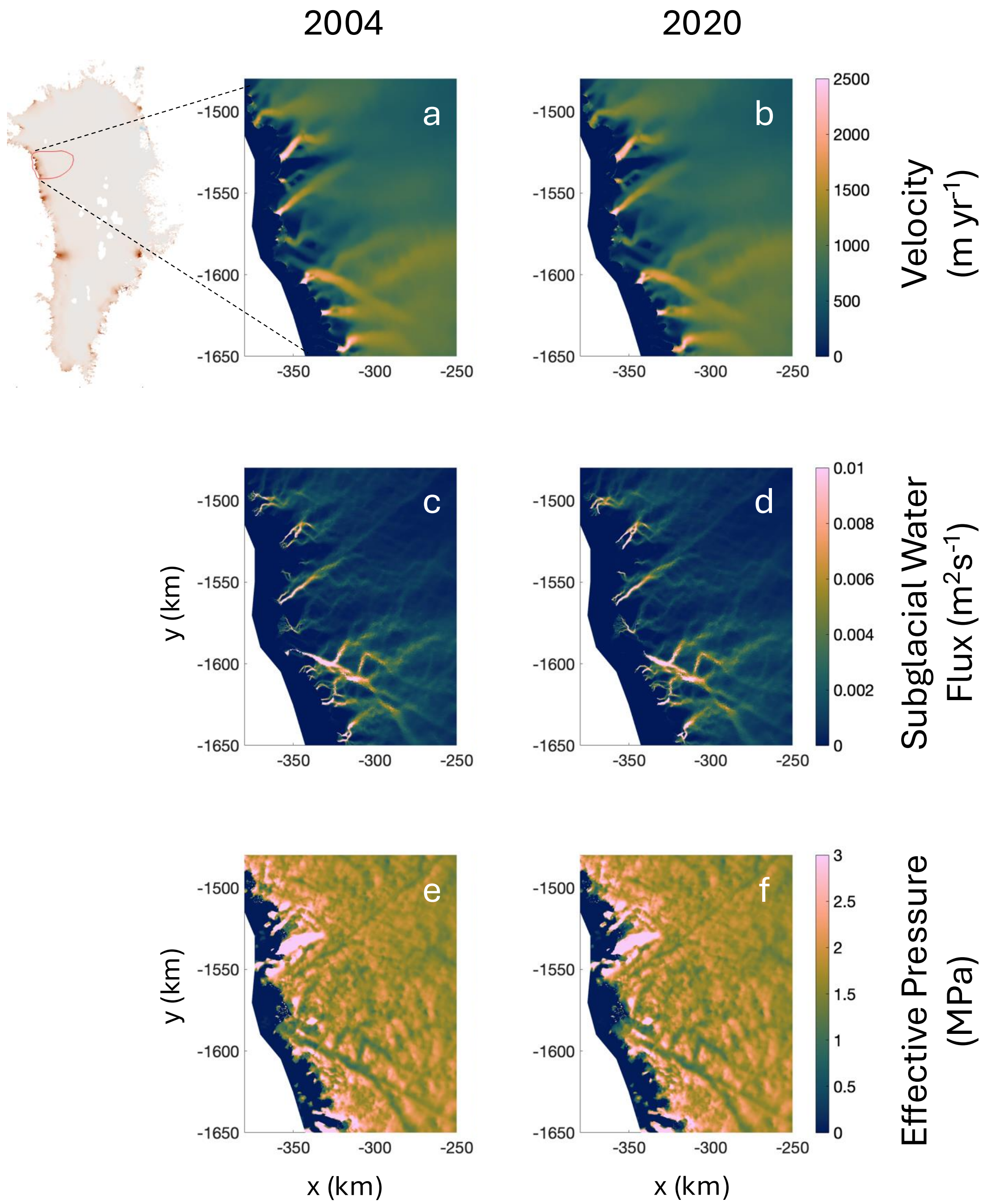

Fig. 1. Model domain in NW Greenland and modeled ice velocity in 2004 (a) and 2020 (b). Modeled subglacial water flux in 2004 (c) and 2020 (d). Modeled effective pressure in 2004 (e) and 2020 (f). All x and y axes are in polar stereographic projection (EPSG: 3413) with units of km.

Ice surface elevation changes

Figure 2a shows the difference in ice surface elevation (2020 - 2004) over the Greenland Ice Sheet as observed by the ICESat and ICESat-2 missions, based on the DEMs described above. Significant elevation decrease (i.e. ice sheet thinning) is visible around the margins of the ice sheet, and no significant increase in surface elevation is apparent. Some major outlet glaciers show large areas of pronounced surface lowering in excess of 100 m over this period, with widespread thinning along the northwest coast. Incremental changes every four years over this period are presented in Figs. S1 and S2, with a general pattern of steady thinning around the ice sheet margins over each segment of time.

Changes in winter water flux, effective pressure, velocity, and basal melt

Figure 2b-g present spatial plots of modeled changes in winter subglacial water flux, effective pressure, ice velocity, and basal melt rate as simulated by the coupled model SHAKTI-ISSM for the ICESat (2004) and ICESat-2 (2020) eras in northwest Greenland, with changes plotted as the difference between these results (2020 minus 2004). Incremental changes every four years over this period are presented in Figs. S2-S5. Changes in subglacial water flow paths caused by changes in surface elevation are clearly visible as blue and red pathways in Fig. 2b. Red indicates a decrease in winter water flux and blue indicates an increase in winter water flux over the period 2004 to 2020. The difference between 2020 and 2004 shows a mix of increases and decreases in water flux at different places. Incremental four-year simulation steps suggest that background water flux generally increased in the interior from 2004 to 2008 with some notable switches in subglacial water flow paths, further reorganized between 2008-2012 and 2012-2016, and experienced more of an overall decrease from 2016-2020 (Fig. S2), resulting in the full mixed reconfiguration apparent in Fig. 2b. For a closer view of the redirection of water flux, percent change in modeled subglacial water flux is shown in Fig. 3a,d, and g for three selected areas.

Modeled effective pressure reveals a consistent decrease in effective pressure near the margin (red), with a general increase in effective pressure in the interior (Fig. 2c). A closer look is provided into percent change in modeled effective pressure in Fig. 3b, e, and h. These changes, however, do not develop through a linear progression, as seen in the four-year incremental change plots in Fig. S3, but rather exhibit more widespread changes in effective pressure during the 2004-2008 and 2016-2020 periods, with relative stability during 2008-2012 and 2012-2016, except for localized increases in effective pressure.

Simulated velocities show deceleration in some outlet glaciers near the margin, while others accelerate,

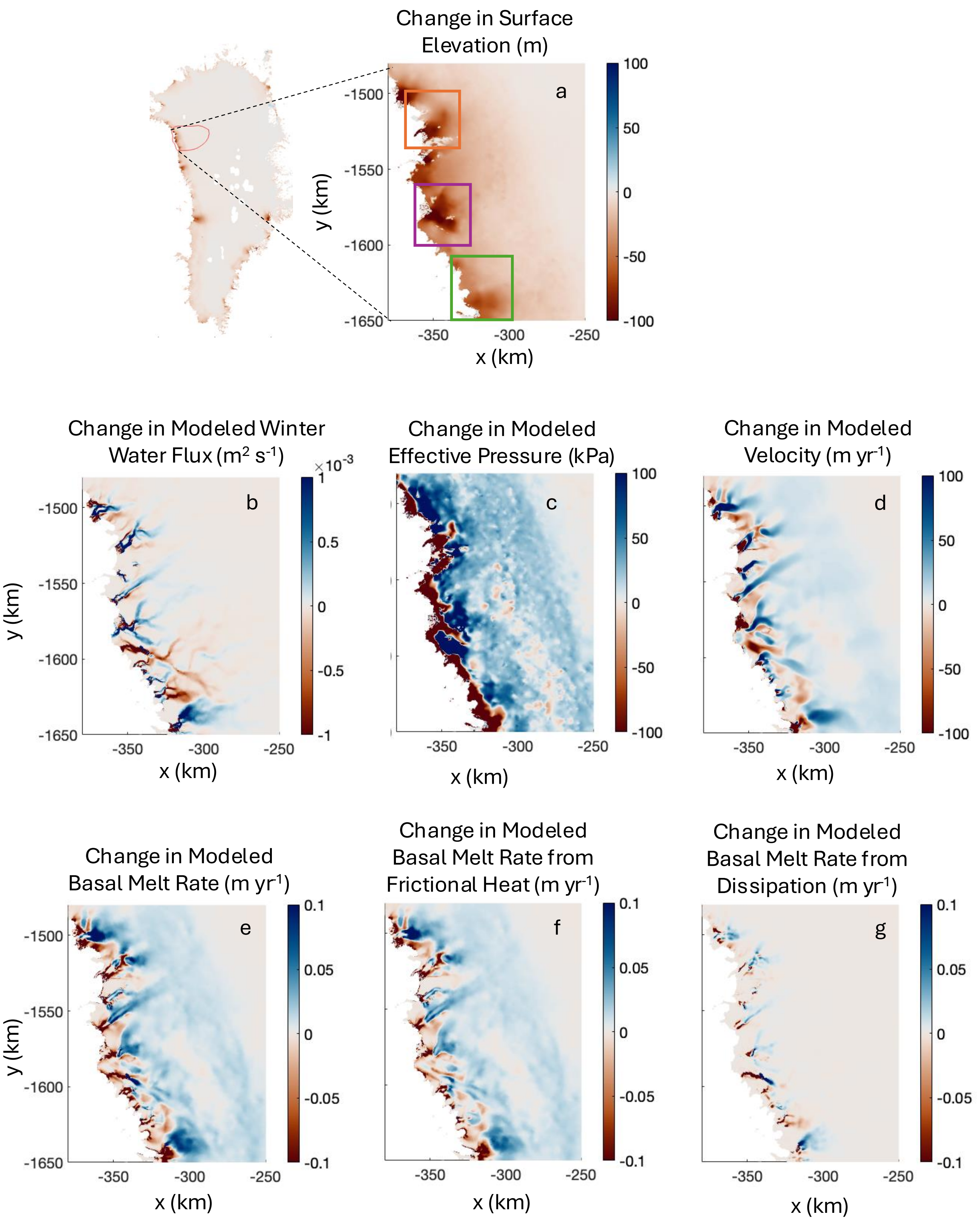

Fig. 2. a) Change in ice surface elevation (2020 minus 2004) over the Greenland Ice Sheet, with model domain in NW Greenland. b-d) Modeled change in background state subglacial water flux (b), effective pressure (c), and ice velocity (d). e-g) Modeled change in total basal melt rate (e) and change in basal melt rate due to frictional heat (f)

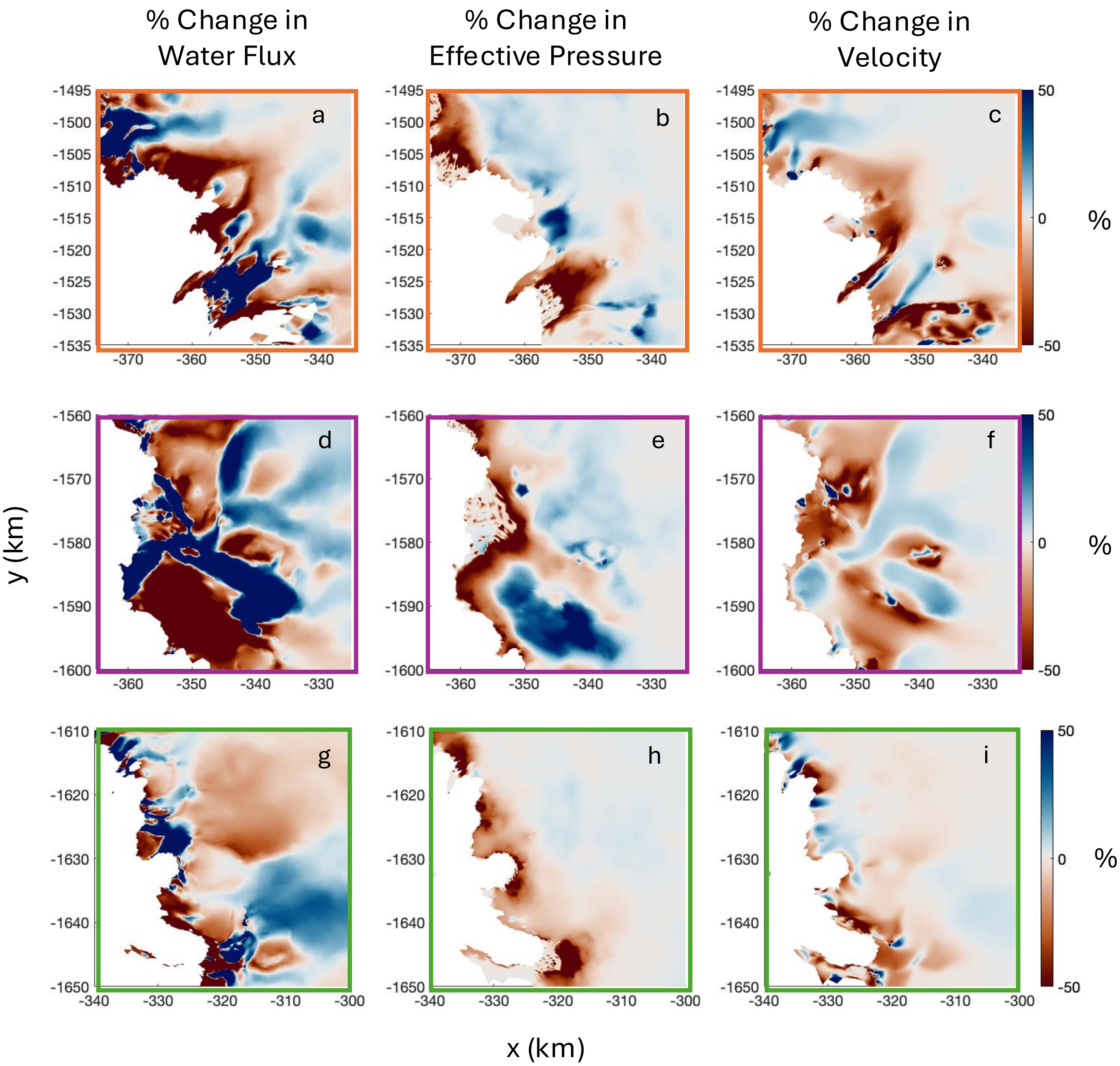

Fig. 3. a) Percent change in modeled background subglacial water flux (a,d,g), effective pressure (b,e,h), and ice velocity (c,f,i) between ICESat (2004) and ICESat-2 (2020) eras, zoomed in for detail in three areas shown on Fig. 2a.

and overall a dominating acceleration trend further inland over the full period 2004 to 2020 (Fig. 2d), with a zoomed in perspective for detail of percent change in velocity in Fig. 3c, f, and i. When viewed over four-year increments, again these patterns of change do not develop linearly over time, but instead show up with mixed acceleration and deceleration during 2004-2008 (Fig. S4). From 2008-2012 and 2012-2016, the modeled velocity change continues to be mixed, with areas of acceleration and deceleration. The period 2016-2020 shows a broad pattern of mild deceleration in the interior with pronounced acceleration in several outlet glaciers.

As calculated by SHAKTI, our simulations suggest a variety of changes in basal melt rate (Fig. 2e) between 2004 and 2020, with locations near the margin experiencing reduced basal melting, and a clear increase in basal melt inland. The bulk of the change in basal melt rate is attributable to changes in frictional heat associated with changes in sliding velocity (Fig. 2f). However, turbulent dissipation corresponding to changes in subglacial water flux is significant at some outlet glaciers, leading to increased basal melt from dissipation in places where winter water flux increased or was redirected (Fig. 2g).

Through examination of changes in ice velocity, effective pressure, basal melt rate, and subglacial water flux as related to changes in ice surface elevation (Fig. 4), a trend emerges relating a decrease in modeled effective pressure with a decrease in surface elevation (Fig. 4b). However, the relationship is weak for predicting changes in modeled velocity or basal melt rate based on changes in surface elevation (Fig. 4a,c,d). An overall relationship between increasing ice velocity and increasing effective pressure is apparent (Fig. 4e). This is perhaps counter-intuitive, as a decrease in effective pressure with ice thinning might be presumed to imply an increase in velocity. The modeled data, however, display a high degree of variability and generally suggest a lack of predictability of ice velocity response to projected ice thinning. We also note that thinner ice does not necessarily imply decreased effective pressure, since the water pressure evolves in response to those changes and does not remain constant, and the ice surface does not lower uniformly everywhere. Coupled simulations such as these provide a window into the nonlinear and complicated behavior of ice sheet dynamics.

Response to seasonal melt

Figure 5 presents time series of mean modeled effective pressure, subglacial water flux, ice velocity, and total basal melt over our model domain in response to seasonal meltwater forcing based on mean 2003-2022 climatology derived from MERRA-2 reanalysis as described above. For both the 2004 and 2020

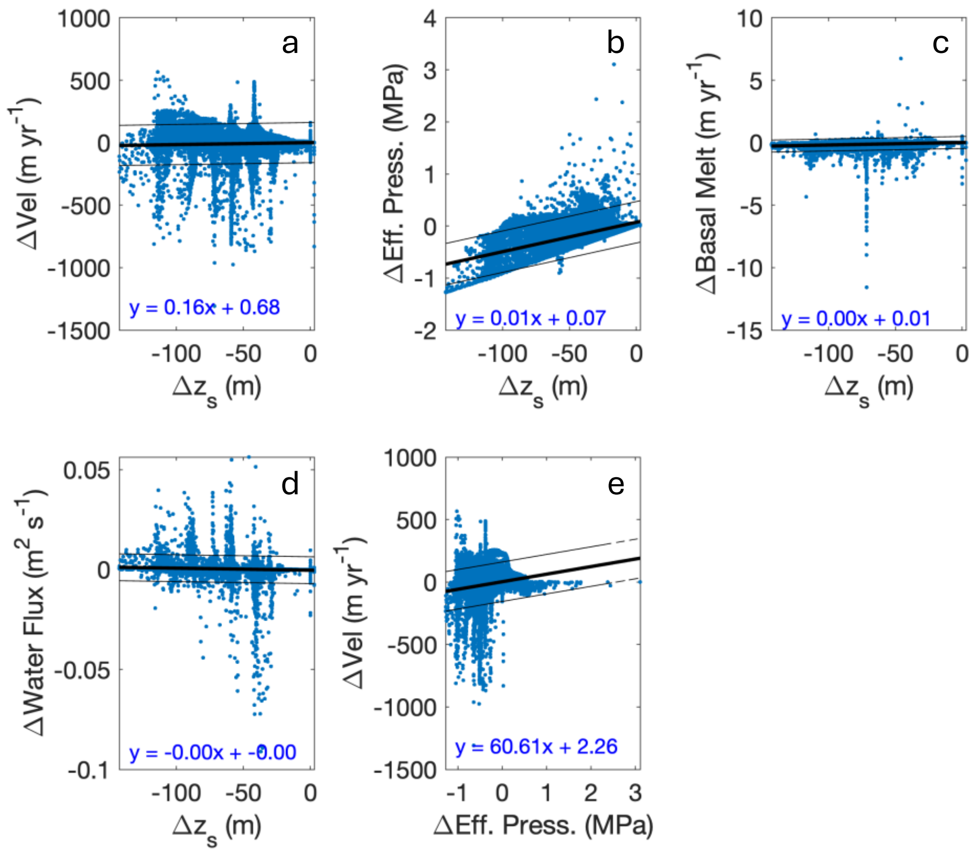

Fig. 4. Change in ice velocity (a), change in effective pressure (b), change in basal melt rate (c), and change in subglacial water flux (d) as a function of change in ice surface elevation. Change in velocity as a function of change in effective pressure (e). Solid dark lines show a linear fit, with ± 95% confidence plotted in light dashed lines.

geometries, subglacial water flux increases during the melt season in response to the runoff inputs. This generally corresponds to an increase in velocity and decrease in effective pressure early in the melt season, followed by deceleration and increase in effective pressure following the peak of the melt season at Day 200. Notably, an abrupt acceleration near the end of the melt season corresponds with a decrease in effective pressure as the drainage system shuts down and becomes less efficient. Overall, the shape of the response is similar in both simulations, but with an offset in effective pressure and velocity between the background winter state for the two eras, reflecting a general decrease in both effective pressure and ice velocity in 2020 as compared to 2004, simply due to the differences in ice surface elevation. While the response is qualitatively similar, the difference between the two seasonal simulations (2020 minus 2004; Fig. 5d-f) reveals some variation around the background offset, with a slightly less negative response in effective pressure during the peak melt season in 2020 compared with 2004, a slightly more negative response in water flux, and a slightly less negative response in velocity. The relationship between the spatial mean modeled quantities in these seasonal simulations using the 2004 and 2020 geometries are plotted in Fig. 5g-i, showing a near-linear pattern, but with some variation around that. These results show that changes in ice geometry and the background subglacial drainage state influence the seasonal response in coupled behavior of the Greenland Ice Sheet, again highlighting the complex response of the ice sheet to changes in surface elevation.

DISCUSSION

Changes in subglacial water flow

Our simulation results show an increase in subglacial water in some areas (appearing blue in Figs. 2b, 3a,d,g) and a reduction in others (appearing red in Figs. 2b, 3a,d,g). The relationship between change in water flux and change in surface elevation is relatively weak when considered over the entire model domain (Fig. 4d). However, some locations suggest an increase in subglacial water being produced and routed toward areas that have experienced enhanced thinning, with a reduction in water flow toward outlets that have maintained relatively more of their thickness (Fig. 2). Local changes in subglacial water flow not only influence ice sliding velocity by changing the pressure distribution at the bed, but also hold ramifications for freshwater discharge into fjords along the margins of the ice sheet. Changes in freshwater flux may have wide-ranging impacts such as changes in fjord circulation patterns, ecology, biogeochemistry, frontal melt rates, and terminus position (Straneo and Cenedese, 2015; Jackson and Straneo, 2016; Sejr and others,

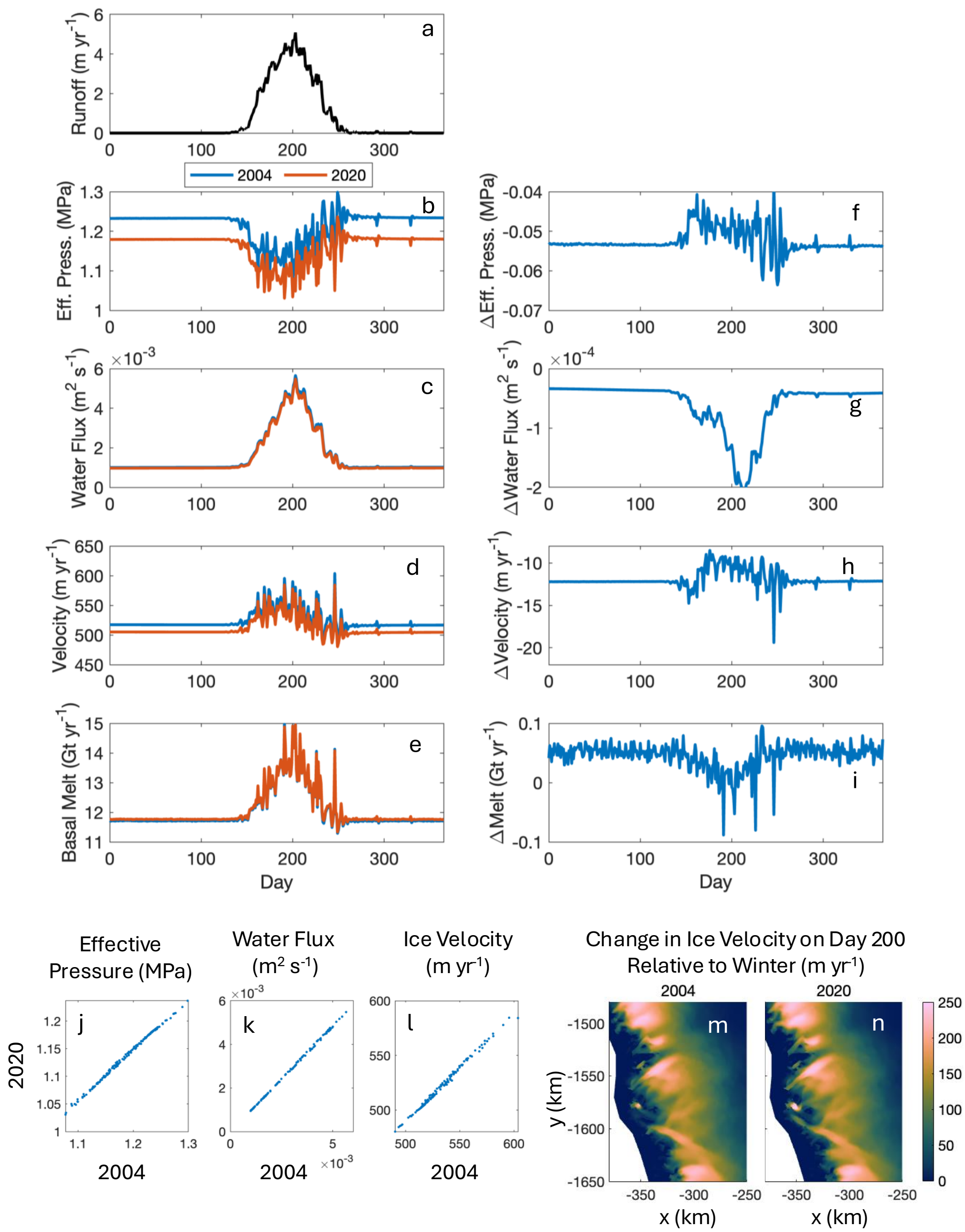

Fig. 5. Mean runoff forcing from 2003-2022 mean MERRA-2 climatology (a), mean modeled effective pressure (b), subglacial water flux (c), ice velocity (d), and total basal melt (e) in response to seasonal meltwater forcing with ice geometry corresponding to the ICESat era (2004; blue) and ICESat-2 era (2020; red). Difference (2020 minus 2004) in mean effective pressure (f), mean subglacial water flux (g), mean ice velocity (h), and total basal melt (i). Relationship of mean effective pressure (j), water flux (k), and velocity (l) between 2004 and 2020 simulations. Change in modeled ice velocity during peak melt season (Day 200) relative to modeled winter ice velocity with 2000 ice elevation (m) and 2020 ice elevation (n).

2022; Vries and others, 2025).

Interior acceleration

We simulate a general decrease in effective pressure near the ice sheet margins, but a modest increase in effective pressure further inland, which corresponds to an overall accelerating trend in simulated winter ice velocity between 2004 and 2020 (Fig. 2c,d). This result may initially seem surprising. If basal conditions remained the same in terms of water pressure, a decrease in ice thickness would lead to a decrease in effective pressure and corresponding acceleration. Our simulations demonstrate a more mixed response. Changes in surface gradients facilitate a reorganization of pressure gradients at the bed that drive the reconfiguration of subglacial water flow and corresponding changes in pressure. These various factors play out in different ways under different specific conditions, and it is worth noting the widespread interior acceleration that occurs even with deceleration in certain locations near the ice sheet margin.

To explore the relative controls on ice velocity changes, we investigate the importance of the redistribution of subglacial water flux (and corresponding changes in effective pressure) as compared to the change in driving stress due to thinning and changing surface slopes. In order to do this, we take the effective pressure distribution resulting from our 2004 simulation, use that effective pressure with the 2020 geometry and calculate the ice velocity from the stress balance under these conditions. The differences in velocity are shown in Fig. S6. While the patterns of change in velocity near the ice-sheet margin are complicated, the interior acceleration is more pronounced in this experiment that separates the control of driving stress changes from the influence of hydrological changes. This suggests that the hydrological impact actually compensates for what would otherwise be larger interior acceleration due to geometry and corresponding driving stress changes alone.

Comparison to velocity observations

We compare our modeled changes in velocity to observed changes in velocity using winter observations derived from synthetic aperture radar (SAR) over the same period. Figure 6 shows the calculated rate of change per year in modeled and observed velocities, and the number of available velocity observations at each location. In general, the model and observations show the same general pattern, with the exception of the very near terminus regions. However, the magnitude of the rate of change is lower in the model than in the observational dataset. Figure 7 shows the percent change in velocity averaged per year over the period

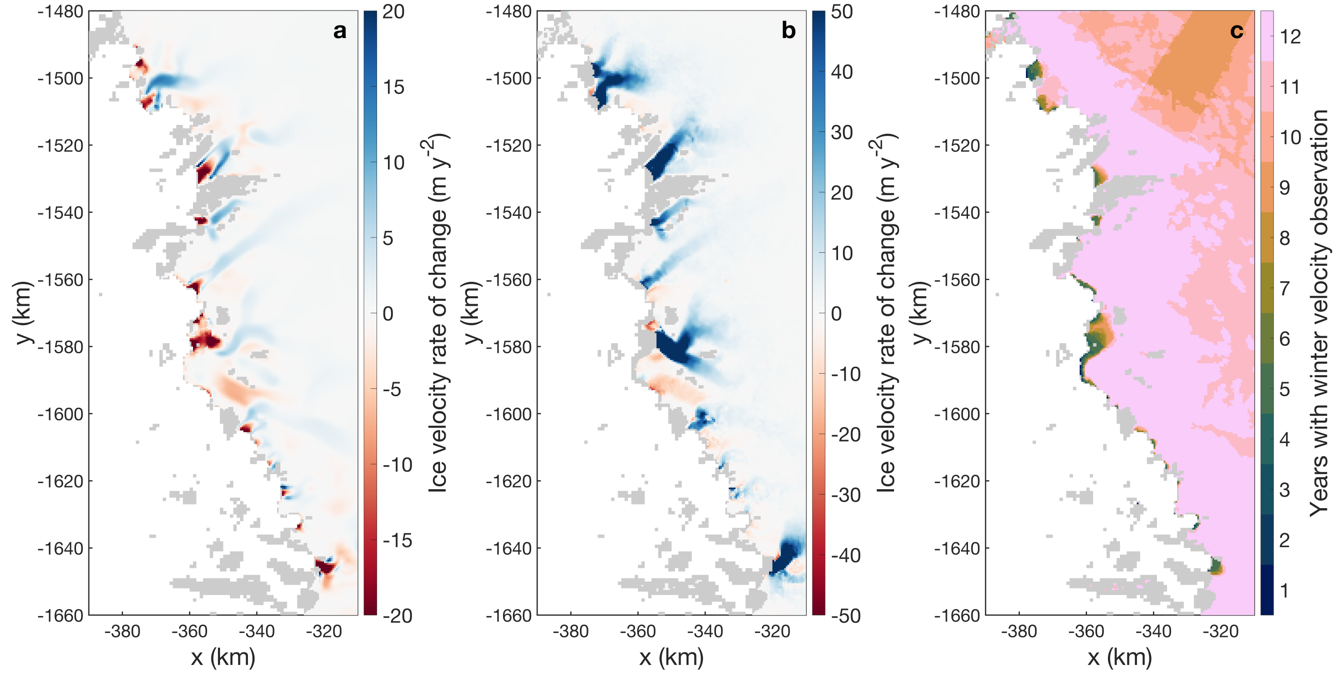

Fig. 6. Rate of change in velocity (2020 minus 2004) as modeled due to change in surface elevation and hydrologic effects (a). Rate of change in observed velocity (b). Count of observations (c).

between 2020 and 2004, as modeled and observed, and the difference between them. The annual trend in mean modeled and observed velocity is presented in Fig. 8, showing a general acceleration. Overall, modeled velocity changes reproduce the correct spatial patterns, but the magnitude of change between 2020 and 2004 is only about 20% of the observed change in velocity. Our winter background modeling approach accounts for changes in surface elevation and changes in subglacial hydrology, isolating these influences from other sources of influence at the terminus such as changes in warm water circulation, changes in terminus position and buttressing support, and other ice/ocean interactions, along with changes in seasonal surface melt. The fact that the model produces velocity changes that generally agree spatially with observations is encouraging, and we interpret this to represent the magnitude of velocity change that can be attributed to changes in ice surface elevation and corresponding changes in the subglacial hydrological system.

Basal melt changes

Ice-sheet mass balance is estimated from melting at the surface, but the ice also melts from below at the ice–bed interface. The role of basal melting has recently been highlighted as an important consideration for overall ice-sheet mass balance (Karlsson and others, 2021; Young and others, 2022), although it is difficult

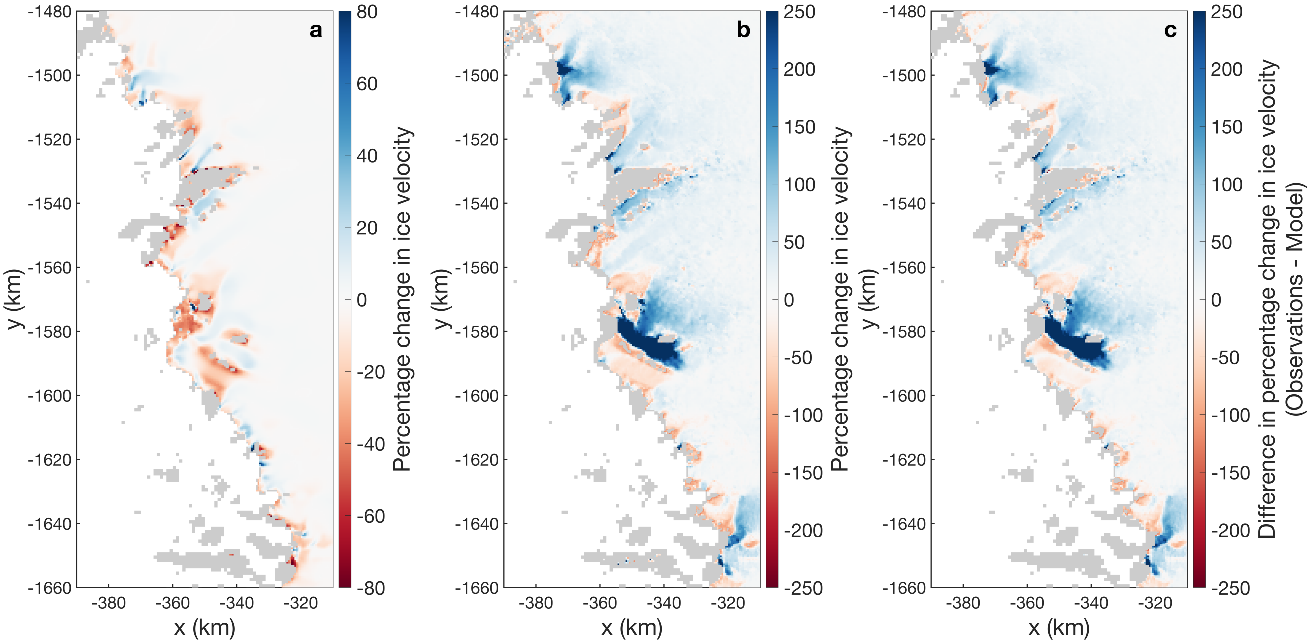

Fig. 7. Percent change in velocity per year as modeled due to change in surface elevation and hydrologic effects (a). Percent change per year in observed velocity (b). Difference between observed and modeled (c).

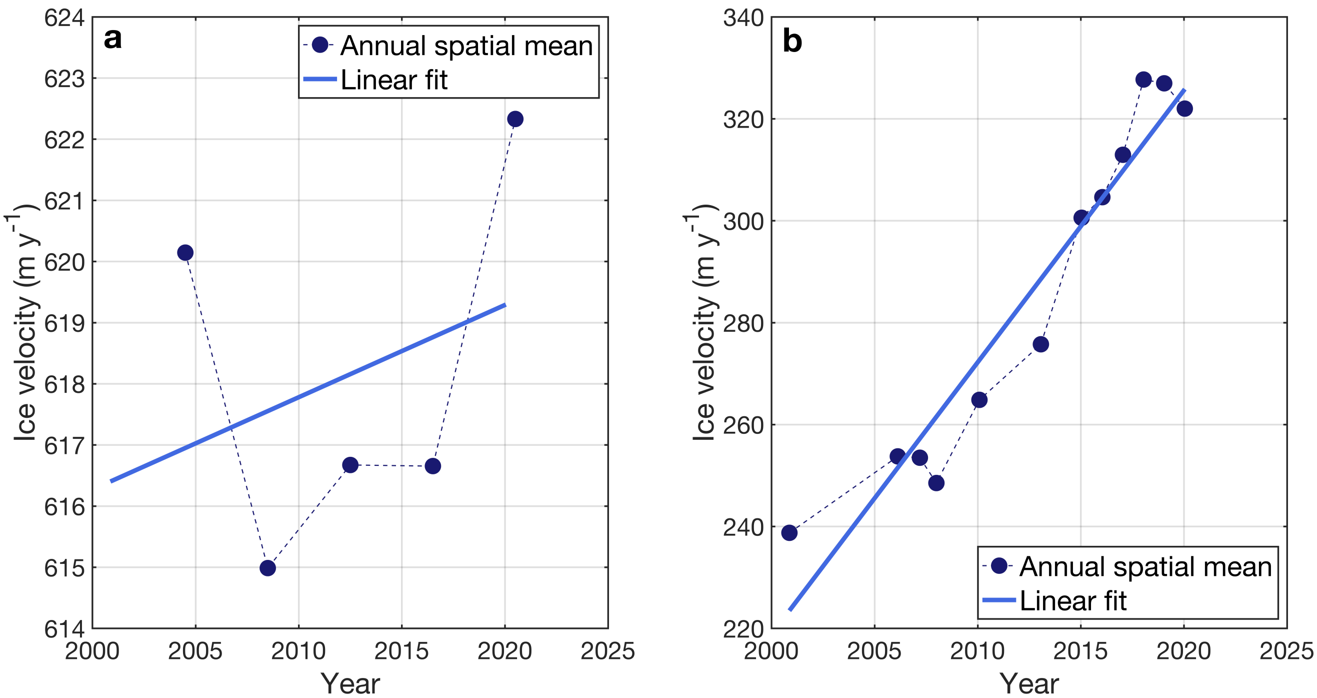

Fig. 8. Mean winter ice velocity and linear regression trend based on modeled (a) and observed (b) velocities.

to observe directly and constrain over large time and space scales. SHAKTI calculates total basal melt rate, along with its components (geothermal, frictional, and turbulent heat), providing an informed estimate of evolving basal melt. As shown in Fig. 2, changes in ice elevation yield heterogeneous changes in basal melt rate in the coupled SHAKTI-ISSM model. In the interior, these changes are dominated by changes in frictional heat, whereas changes in dissipation are important at the outlets, especially in places where subglacial water flux has increased or decreased through hydrologic reorganization as a result of changes in surface elevation.

Our coupled winter simulations calculate a total background basal melt volume over our model domain of 11.72 Gt yr^{-1} in 2004 and 11.77 Gt yr^{-1} in 2020. This implies an increase of 0.05 Gt yr^{-1} in background basal melt in this region.

Importance of the winter background state

Changes in ice surface elevation alone alter the pattern of basal melting and, over the 2004 to 2020 interval, result in substantial changes in the subglacial winter background state. Our seasonal simulation results (Fig. 5) suggest that the winter background state has a non-negligible influence in determining pressure and velocity magnitudes. The winter background state is determined by ice geometry that has shifted over time on a decadal scale between the eras of ICESat and ICESat-2 observations. It is notable that the seasonal pressure and velocity responses in our seasonal simulations using 2004 and 2020 geometries are offset based on the winter background state when forced with the same transient runoff inputs to the bed, but also exhibit differences in the magnitude of response during the melt season (Fig. 5). While in reality, seasonal forcing evolves over time and also exhibits interannual variability, this modeled exercise allows for isolation of the difference in response due to geometry alone. It is also perhaps unexpected that the ICESat-2 era displays both a decrease in mean modeled effective pressure and mean modeled velocity, as one might expect that a decrease in effective pressure should lead to increased velocity. The key here is that these quantities are mean values over the entire domain; although our simulations produce an increase in effective pressure in the interior, we calculate substantial decreases in effective pressure along the margins, which act to significantly lower the mean value of change in effective pressure. These findings demonstrate the complex impact of changes in surface elevation and the resulting response in ice dynamics, when accounting for the coupled effects of subglacial hydrology.

Limitations

As in any modeling effort, we made informed choices of parameter values and approximations to physics, including choices for ice temperature and rheology, flow law approximation, sliding law, process parameterizations, and forcing data. We cannot and do not aim to perfectly reproduce reality with all its complexities, but we do aspire to represent the relevant physical processes in an appropriate way to assess feedbacks and make inferences about realistic behavior of the Greenland Ice Sheet. In the landscape of coupled subglacial hydrology and ice dynamics modeling, much remains for future work to rigorously assess the impact of different sliding laws and improve parameterization of basal friction with evolving hydrology. For example, McArthur and others (2023) found that the Schoof friction law produced better velocity results than the Budd friction law in coupled modeling of an Antarctic glacier using a different subglacial hydrology model, and Meyer and others (2026) compared coupled simulations using SHAKTI-ISSM with both Budd and Schoof friction laws at Thwaites Glacier at Thwaites Glacier.

At least in the early part of our study period (2004-09), the resolution of our elevation-change maps is limited by the track-to-track spacing of the ICESat data, which is up to 20 km in the southern part of our domain. This means that the elevation-change estimates may not resolve the fine details of surface-elevation change, and may underestimate gradients in elevation change around relatively small topographic features such as outlet glaciers.

We selected our model domain in northwest Greenland based on its significant widespread surface elevation change between 2004 and 2020, representative of the ICESat and ICESat-2 eras (Fig. 2a). Future research should model larger regions of the Greenland Ice Sheet, ideally the entire ice sheet. The work presented here represents advances in coupled subglacial hydrology–ice dynamics modeling using SHAKTI-ISSM on a larger domain than previous applications to single glaciers. Further work should aim to expand these modeling capabilities and establish robust general boundary conditions that can easily be applied to any complicated ice sheet or glacier domain. Moreover, much remains to be explored regarding how best to represent sliding laws and geological friction coefficients while modeling coupled ice velocity and subglacial hydrology.

CONCLUSIONS

In this study, we present large-scale coupled subglacial hydrology and ice dynamics using SHAKTI and ISSM applied to northwest Greenland. We find that changes in ice surface elevation, as observed by satellite laser altimetry from NASA's ICESat and ICESat-2 missions and derived gridded products, yield changes in subglacial water flow and corresponding ice velocity, along with changes in basal melt rates. We find instances of increased subglacial water flow toward outlets with enhanced thinning and decreased water flow toward outlets that have retained more of their ice thickness. This reorganization of freshwater discharge holds potential impacts for fjord dynamics, biogeochemistry, and ecology, as well as for frontal ablation rates (including both melt and calving processes). Our simulations demonstrate decreased effective pressure and locations of decreased ice velocity near the margins of the ice sheet, but conversely a modest increase in effective pressure and overall velocity acceleration in the interior. Compared to the observed velocity changes during this period, our coupled model suggests that changes in surface elevation and subglacial hydrology contribute approximately 20% of the total observed velocity change as modeled here, without accounting for changes in terminus forcing (i.e. changes in terminus position, buttressing, warm water circulation in fjords, etc.). Accompanied by an increase in simulated background basal melt rate, these results suggest feedbacks intensifying mass loss from the Greenland Ice Sheet attributable to changes in ice surface elevation and changes in the subglacial system. Changing the geometry alone yields a higher interior acceleration due to changes in driving stress than with coupled hydrological changes, indicating that the impacts from changing hydrology and basal stress help to soften the inland acceleration effect of changes in driving stress.. The coupled simulations demonstrate the complexity and nuance in accounting for changes in effective pressure due to changes in subglacial hydrology, while highlighting how the ice sheet and its subglacial drainage system respond heterogeneously to changes in surface elevation.

ACKNOWLEDGMENTS

This study was supported by NASA grants 80NSSC23K1329 and 80NSSC23K0937. We thank Ian Hewitt and the reviewers for their helpful comments.

DATA AVAILIABILITY

We used ISSM version 4.24. ISSM (including SHAKTI) is freely and publicly available for download at https://github.com/ISSMteam/ISSM. Model output data and code are available in a permanent Zenodo archive (DOI: 10.5281/zenodo.21266719).

REFERENCES

Abdalati W, Zwally HJ, Bindschadler R, Csatho B, Farrell SL, Fricker HA, Harding D, Kwok R, Lefsky M, Markus T, Marshak A, Neumann T, Palm S, Schutz B, Smith B, Spinhirne J and Webb C (2010) The ICESat-2 laser altimetry mission. *Proceedings of the IEEE*, **98**(5), 735–751 (doi: 10.1109/JPROC.2009.2034765)

Andrews LC, Catania GA, Hoffman MJ, Gulley JD, Lüthi MP, Ryser C, Hawley RL and Neumann TA (2014) Direct observations of evolving subglacial drainage beneath the Greenland Ice Sheet. *Nature*, **514**(7520), 80–83 (doi: 10.1038/nature13887)

Badgeley JA, Morlighem M and Seroussi H (2025) Increased sea-level contribution from northwestern Greenland for models that reproduce observations. *Proceedings of the National Academy of Sciences*, **122**(25), e2411904122 (doi: 10.1073/pnas.2411904122)

Banwell A, Hewitt I, Willis I and Arnold N (2016) Moulin density controls drainage development beneath the Greenland Ice Sheet. *Journal of Geophysical Research: Earth Surface*, **121**(12), 2248–2269 (doi: 10.1002/2016JF003764)

Budd W, Keage P and Blundy N (1979) Empirical studies of ice sliding. *Journal of Glaciology*, **23**(89), 157–170 (doi: 10.3189/S0022143000029804)

Cowton T, Nienow P, Sole A, Bartholomew I and Mair D (2016) Variability in ice motion at a land-terminating Greenlandic outlet glacier: the role of channelized and distributed drainage systems. *Journal of Glaciology*, **62**(233), 451–466 (doi: 10.3189/2016JoG61.021)

Flowers GE (2015) Modelling water flow under glaciers and ice sheets. *Proceedings of the Royal Society A: Mathematical, Physical and Engineering Sciences*, **471**(2176), 20140907 (doi: 10.1098/rspa.2014.0907)

Gelaro R, McCarty W, Suárez MJ, Todling R, Molod A, Takacs L, Randles CA, Darmenov A, Bosilovich MG, Reichle R and others (2017) The modern-era retrospective analysis for research and applications, version2 (MERRA-2). *Journal of Climate*, **30**(14), 5419–5454 (doi: 10.1002/joc.5089)

Hanna E, Navarro FJ, Pattyn F, Domingues CM, Fettweis X, Ivins ER, Nicholls RJ, Ritz C, Smith B, Tulaczyk S and others (2013) Ice-sheet mass balance and climate change. *Nature*, **498**(7452), 51–59 (doi: 10.1038/nature12211)

Jackson RH and Straneo F (2016) Heat, salt, and freshwater budgets for a glacial fjord in Greenland. *Journal of Physical Oceanography*, **46**(9), 2735–2768 (doi: 10.1175/JPO-D-15-0186.1)

Joughin I (2023) MEaSUREs Greenland quarterly ice sheet velocity mosaics from SAR and Landsat, Version5. *Boulder, Colorado, USA. NASA National Snow and Ice Data Center Distributed Active Archive Center* (doi: 10.5067/V5KW64S63OSN)

Joughin I, Smith BE, Howat IM, Scambos T and Moon T (2010) Greenland flow variability from ice-sheet-wide velocity mapping. *Journal of Glaciology*, **56**(197), 415–430 (doi: 10.3189/2010JoG56.021)

Joughin I, Smith B, Howat I and Scambos T (2015) MEaSUREs Greenland Ice Sheet velocity map from InSAR data, version2 (doi: 10.5067/OC7B04ZM9G6Q)

Joughin I, Smith BE and Howat I (2018) Greenland ice mapping project: ice-flow velocity variation at sub-monthly to decadal timescales. *The Cryosphere*, **12**(7), 2211–2227 (doi: 10.5194/tc-12-2211-2018)

Karlsson NB, Solgaard AM, Mankoff KD, Gillet-Chaulet F, MacGregor JA, Box JE, Citterio M, Colgan WT, Larsen SH, Kjeldsen KK and others (2021) A first constraint on basal melt-water production of the Greenland Ice Sheet. *Nature Communications*, **12**(1), 1–10 (doi: 10.1038/s41467-021-21349-5)

Larour E, Seroussi H, Morlighem M and Rignot E (2012) Continental-scale, high-order, high-spatial-resolution ice-sheet modelling using the Ice Sheet System Model (ISSM). *Journal of Geophysical Research: Earth Surface*, **117**(F1) (doi: 10.1029/2011JF002140)

MacAyeal DR (1989) Large-scale ice flow over a viscous basal sediment: theory and application to Ice Stream B, Antarctica. *Journal of Geophysical Research: Solid Earth*, **94**(B4), 4071–4087 (doi: 10.1029/JB094iB04p04071)

MacGregor JA, Boisvert LN, Medley B, Petty AA, Harbeck JP, Bell RE, Blair JB, Blanchard-Wrigglesworth E, Buckley EM, Christoffersen MS, Cochran JR, Csathó BM, De Marco EL, Dominguez RT, Fahnestock MA, Farrell SL, Gogineni SP, Greenbaum JS, Hansen CM, Hofton MA, Holt JW, Jezek KC, Koenig LS, Kurtz NT, Kwok R, Larsen CF, Leuschen CJ, Locke CD, Manizade SS, Martin S, Neumann TA, Nowicki SM, Paden JD, Richter-Menge JA, Rignot EJ, Rodríguez-Morales F, Siegfried MR, Smith BE, Sonntag JG, Studinger M, Tinto KJ, Truffer M, Wagner TP, Woods JE, Young DA and Yungel JK (2021) The scientific legacy of nasa's operation icebridge. *Reviews of Geophysics*, **59**(2), e2020RG000712 (doi: https://doi.org/10.1029/2020RG000712), e2020RG000712 2020RG000712

Mankoff KD, Solgaard A, Colgan W, Ahlström AP, Khan SA and Fausto RS (2020) Greenland Ice Sheet solid ice discharge from 1986 through march 2020. *Earth System Science Data*, **12**(2), 1367–1383 (doi: 10.5194/essd-12-1367-2020)

Markus T, Neumann T, Martino A, Abdalati W, Brunt K, Csatho B, Farrell S, Fricker H, Gardner A, Harding D, Jasinski M, Kwok R, Magruder L, Lubin D, Luthcke S, Morison J, Nelson R, Neuenschwander A, Palm S, Popescu S, Shum C, Schutz B, Smith B, Yang Y and Zwally J (2017) The Ice, Cloud, and land Elevation Satellite-2 (ICESat-2): science requirements, concept, and implementation. *Remote Sensing of Environment*, **190**, 260–273 (doi: 10.1016/j.rse.2016.12.029)

McArthur K, McCormack FS and Dow CF (2023) Basal conditions of Denman Glacier from glacier hydrology and ice dynamics modeling. *The Cryosphere*, **17**(11), 4705–4727 (doi: 10.5194/tc-17-4705-2023)

Meierbachtol T, Harper J and Humphrey N (2013) Basal drainage system response to increasing surface melt on the Greenland Ice Sheet. *Science*, **341**(6147), 777–779 (doi: 10.1126/science.1240175)

Meyer CR and Hewitt IJ (2017) A continuum model for meltwater flow through compacting snow. *Cryosphere*, **11**(6), 2799–2813 (doi: 10.5194/tc-11-2799-2017)

Meyer CR, Warburton KL, Sommers AN and Minchew BM (2026) A model of water extraction from the subglacial hydrologic system under idealized conditions. *The Cryosphere*, **20**(5), 2659–2680 (doi: 10.5194/tc-20-2659-2026)

Morlighem M and others (2021) IceBridge BedMachine Greenland, version 4 [data set]. *NASA National Snow and Ice Data Center Distributed Active Archive Center* (doi: 10.5067/VLJ5YXKCNGXO)

Mouginot J, Rignot E, Bjørk AA, Van den Broeke M, Millan R, Morlighem M, Noël B, Scheuchl B and Wood M (2019) Forty-six years of Greenland Ice Sheet mass balance from 1972 to 2018. *Proceedings of the National Academy of Sciences*, **116**(19), 9239–9244 (doi: 10.1073/pnas.1904242116)

Rada Giacaman CA and Schoof C (2023) Channelized, distributed, and disconnected: spatial structure and temporal evolution of the subglacial drainage under a valley glacier in the Yukon. *The Cryosphere*, **17**(2), 761–787 (doi: 10.5194/tc-17-761-2023)

Rennermalm , Hock R, Covi F, Xiao J, Corti G, Kingslake J, Leidman SZ, Miège C, Macferrin M, Machguth H and others (2022) Shallow firn cores 1989–2019 in southwest Greenland's percolation zone reveal decreasing density and ice layer thickness after 2012. *Journal of Glaciology*, **68**(269), 431–442 (doi: 10.1017/jog.2021.107)

Schoof C (2005) The effect of cavitation on glacier sliding. *Proceedings of the Royal Society A: Mathematical, Physical and Engineering Sciences*, **461**(2055), 609–627 (doi: 10.1098/rspa.2005.1626)

Schoof C (2010) Ice-sheet acceleration driven by melt supply variability. *Nature*, **468**(7325), 803–806 (doi: 10.1038/nature09566)

Schutz BE, Zwally HJ, Shuman CA, Hancock D and DiMarzio JP (2005) Overview of the ICESat mission. *Geophysical Research Letters*, **32**(21), L21701 (doi: 10.1029/2005GL024009)

Sejr MK, Bruhn A, Dalsgaard T, Juul-Pedersen T, Stedmon CA, Blicher M, Meire L, Mankoff KD and Thyrring J (2022) Glacial meltwater determines the balance between autotrophic and heterotrophic processes in a Greenland fjord. *Proceedings of the National Academy of Sciences*, **119**(52), e2207024119 (doi: 10.1073/pnas.2207024119)

Shepherd A, Ivins ER, A G, Barletta VR, Bentley MJ, Bettadpur S, Briggs KH, Bromwich DH, Forsberg R, Galin N and others (2012) A reconciled estimate of ice-sheet mass balance. *Science*, **338**(6111), 1183–1189 (doi: 10.1126/science.1226236)

Simkins LM, Greenwood SL, Munevar Garcia S, Eareckson EA, Anderson JB and Prothro LO (2021) Topographic controls on channelized meltwater in the subglacial environment. *Geophysical Research Letters*, **48**(20), e2021GL094678 (doi: 10.1029/2021GL094678)

Smith B, Fricker HA, Holschuh N, Gardner AS, Adusumilli S, Brunt KM, Csatho B, Harbeck K, Huth A, Neumann T and others (2019) Land ice height-retrieval algorithm for NASA's ICESat-2 photon-counting laser altimeter. *Remote Sensing of Environment*, **233**, 111352 (doi: 10.1016/j.rse.2019.111352)

Smith B, Jelley BP, Dickinson S, Sutterley T, Neumann T and Harbeck K (2025) Atlas/icesat-2 l3b gridded antarctic and greenland height change, version 5 (doi: 10.5067/ATLAS/ATL15.005)

Smith B, Sutterley TC, Fricker HA, Padman L, Siegfried MR, Black T, Felikson D, Freer BID, Gibbons A, Howard SL and et al (2026) Icesat-2 land ice products resolve greenland and antarctic ice-sheet height changes on seasonal to multiyear time scales. *Journal of Glaciology*, 1–55 (doi: 10.1017/jog.2026.10152)

Smith LC, Chu VW, Yang K, Gleason CJ, Pitcher LH, Rennermalm , Legleiter CJ, Behar AE, Overstreet BT, Moustafa SE and others (2015) Efficient meltwater drainage through supraglacial streams and rivers on the southwest Greenland Ice Sheet. *Proceedings of the National Academy of Sciences*, **112**(4), 1001–1006 (doi: 10.1073/pnas.1416537112)

Sommers A, Rajaram H and Morlighem M (2018) SHAKTI: subglacial hydrology and kinetic, transient interactions v1.0. *Geoscientific Model Development*, **11**(7), 2955–2974 (doi: 10.5194/gmd-11-2955-2018)

Sommers A, Meyer C, Morlighem M, Rajaram H, Poinar K, Chu W and Mejia J (2023) Subglacial hydrology modelling predicts high winter water pressure and spatially variable transmissivity at Helheim Glacier, Greenland. *Journal of Glaciology*, **69**(267), 1–13 (doi: 10.1017/jog.2023.39)

Sommers AN, Meyer CR, Poinar K, Mejia J, Morlighem M, Rajaram H, Warburton KLP and Chu W (2024) Velocity of Greenland's Helheim Glacier controlled both by terminus effects and subglacial hydrology with distinct realms of influence. *Geophysical Research Letters*, **51**(15), e2024GL109168 (doi: 10.1029/2024GL109168)

522 Straneo F and Cenedese C (2015) The dynamics of Greenland's glacial fjords and their role in climate. *Annual Review of Marine Science*, **7**(1), 89–112 (doi: 10.1146/annurev-marine-010814-015944)

524 Sundal AV, Shepherd A, Nienow P, Hanna E, Palmer S and Huybrechts P (2011) Melt-induced speed-up of Greenland Ice Sheet offset by efficient subglacial drainage. *Nature*, **469**(7331), 521–524 (doi: 10.1038/nature09701)

526 Vries AL, van de Berg WJ, Noël B, Meire L and van den Broeke MR (2025) Seasonal and interannual variability in freshwater sources for Greenland's fjords. *The Cryosphere*, **19**(9), 3897–3914 (doi: 10.5194/tc-19-3897-2025)

528 Warburton KLP, Meyer CR and Sommers AN (2024) Predicting the onset of subglacial drainage channels. *Journal of Geophysical Research: Earth Surface*, **129**(12), e2024JF007758 (doi: 10.1029/2024JF007758)

530 Young T, Christoffersen P, Bougamont M, Tulaczyk S, Hubbard B, Mankoff K, Nicholls K and Stewart C (2022) Rapid basal melting of the Greenland Ice Sheet from surface meltwater drainage. *Proceedings of the National Academy of Sciences*, **119**(10), e2116036119 (doi: 10.1073/pnas.2116036119)

Supplementary Information for "Ice Surface Change Drives Interior Slowdown and Hydrologic Reorganization in Northwest Greenland"

Aleah SOMMERS,[1] Aaron STUBBLEFIELD,[2,3] Lauren ANDREWS,[3] Colin R. MEYER,[1] Benjamin E. SMITH[4]

[1] *Thayer School of Engineering, Dartmouth College, Hanover, NH, USA*

[2] *University of Maryland, College Park, MD, USA*

[3] *NASA Goddard Space Flight Center, Greenbelt, MD, USA*

[4] *Applied Physics Laboratory, University of Washington, Seattle, WA, USA*

Correspondence: Aleah Sommers <aleah.n.sommers@dartmouth.edu>

Contents of this file:

1. DEM methods
2. Tables S1 to S2
3. Figures S1 to S6

DEM METHODS

Reference DEM estimation

To generate the 2020.5 reference DEM, we used the algorithm used to generate the ICESat-2 ATL14/15 product (Smith and others, 2025b, 2026), modified in three main ways::

1. ICEsat-2 data source: Instead of the ATL11 (along-track slope-corrected height, Smith and others (2025a))product, the algorithm used here uses the higher-resolution ATL06 along-track height product (Smith and others, 2019). This allows the ICESat-2 measurements to match the resolution of the ArcticDEM product.

2. ArcticDEM elevation products: To help resolve small-scale topography between ICESat-2 tracks, we include ArcticDEM DEM strips (Porter and others, 2022). These strips provide elevations at 2-m resolution, with near-complete repeat coverage of Greenland 1-2 times per year. We filter and subsample each strip to 32-m resolution, and assign each pixel an estimated uncertainty equal to the RSS (root sum of squares) of a 5-m horizontal geolocation uncertainty times the surface slope, and the RMS difference between pixel's elevation and the elevations of the surrounding pixels in the 2-m input DEM (accumulated using a 32-m Gaussian average). During the surface-fitting process, we solve for an additional set of parameters for each DEM to account for across-track stripe artifacts that result from misalignment of satellite sensor pixels (Shean and others, 2016), and along-track artifacts that sometimes appear in the DEMs, possibly due to imperfections in the sensor geolocation models (similar to Girod and others (2015)). These corrections take the form of one piecewise-linear function with 100-m node spacing in the across-track direction and a second piecewise-linear linear function with 500-m resolution in the along-track direction, where the along-and across-track directions are determined separately for each strip. The coefficients of these functions are determined during the least-track fitting procedure along with the DEM and height-change parameters. We also solve for the uniform per-strip 5-m-RMS vertical elevation bias that has been observed in similar DEMs (Shean and others, 2019).

3. Firn-air and surface-mass-balance correction We correct for expected surface-elevation variations driven by snowfall and compaction by subtracting a model that estimates height changes due to accumulation and firn-air content change (Medley and others, 2022). We subtract the sum of the firn-air-content anomaly and the ice-accumulation anomaly from each measured elevation before fitting, then add the ice-accumulation anomaly to the estimated DEM and elevation-change surfaces. These steps are intended to reduce the sampling error that can arise when altimetry data do not evenly sample the seasonal variations in the ice-sheet surface elevation.

We apply the fitting algorithm to ICESat-2 and ArcticDEM data spanning 1 January 2019 - 31 December 2023, and solve for a reference DEM for July 1 2020 with a horizontal posting of 50 m and a set of elevation-change surfaces with 0.25-a temporal and 500-m horizontal posting.

We perform the calculations on overlapping 18-km tiles, with tile centers separated by 10 km, and mosaick the final products from these tiles using a cosine-taper weighting function in the overlapping regions. We do not use the elevation-change surfaces ($\delta(x, y, t)$) in the current study, but need to include them in the solution to allow data from multiple temporal epochs to contribute to the DEM surface. The result of this procedure is a nearly seamless map of Greenland elevations that includes data that resolve fine-scale surface features almost everywhere on the ice sheet. There are a few regions in south-central Greenland where high-quality ArcticDEM data were not available during our study period; in these areas, we marked the pixels directly sampled by ICESat-2 (with 200-m tolerance) as valid, and marked the unconstrained pixels as invalid.

Decadal elevation-change estimates

To estimate elevation surfaces for 2004, 2008, 2012, and 2016, we apply the surface-fitting algorithm to the differences between laser-altimetry data spanning 2004-2019 and the reference 2020.5 DEM. We use release 634 ICESat data (Zwally and others, 2014), ATM (Airborne Topographic Mapping system) ICESSN data (Studinger, 2014), and LVIS (Laser Vegetation and Ice measurement System) geolocated surface elevation product (Blair and Hofton, 2019). The scanning laser altimetry datasets provide data over a swath beneath the aircraft, and we have found that in some cases small errors in the instrument orientation can produce artificial tilts in the data which appear in the gridded product as gradients in elevation change. We avoid this effect by using only a narrow swath of data beneath the instrument. For the ATM data, which reduces the instrument's point cloud to a set of planar facets, we select only the near-nadir facet. For LIVS, we select only the elevation measurements that fell within 50 m of the center of the swath. We convert each product to the ITRF2014 reference system, relative to the WGS84 ellipsoid, and because our goal is to create a time-varying surface-elevation estimate for the ice sheet (rather than mass change) we do not correct for the effects of glacial isostatic adjustment or elastic rebound.

We fit a time series of elevation changes to the subsampled pre-ICESat-2 elevation measurements by subtracting 2020.5 DEM from each measurement, then fitting the elevation residuals with a smoothly varying surface, on a 500-m horizontal, 1-yr temporal grid:

$$\delta_{pre} = fmin_{\delta_{pre}} \left(\sum_{data} \left(\frac{\delta_{pre} - (z_i - z_{DEM} - b_i - \delta_{SMB,i} - \delta_{FAC,i}}{\sigma_i} \right)^2 + W_{xxt} \int \nabla^2 \partial_t \delta_{pre} dAdt + \sum_{biases} \left(\frac{b_j}{E(b_j)} \right)^2 \right)$$

Here W_{xxt} is a weighting function that describes the importance of model smoothness in the solution relative to data misfit, b_j represents the biases for each dataset, and $E(b_j)$ is the expected RMS bias for the dataset; we assume that each dataset has a unique bias value for each day, with an expected RMS variability of 0.03 m. Solving for uncertain bias values in this way lets us take into account the effects of correlated errors in the data. We solve for the decadal elevation change on overlapping 40-km tiles, whose centers are spaced 10 km apart, then mosaic these tiles using a raised-cosine weighting function.

Constructing the elevation time series

We derive elevations for the DEMs by adding the SMB anomaly to the sum of the DEM and the height-change maps:

$$z(x, y, t) = z_{2020.5}(x, y) + \delta_p rex, y, t + \delta_{SMB} x, y, t$$

This estimate essentially copies the details of the surface topography in the 2019 DEM to the previous years, using the coarser-resolution elevation-change maps derived from IceBridge and ICESat to constrain the larger-scale changes in ice-sheet topography driven by patterns of ice-sheet mass imbalance.

Table 1. Constants and parameter values used in this study

Symbol	Value	Units	Description
A	3.5×10^{-25}	$Pa^{-3}\ s^{-1}$	Flow law parameter (for ice at -10°C)
C	Spatially varying	$s^{1/2}\ m^{-1/2}$	Drag coefficient used in basal stress calculation
G	Spatially varying 0.04-0.06	$W\ m^{-2}$	Geothermal flux (Shapiro and Ritzwoller, 2004)
g	9.81	$m\ s^{-2}$	Gravitational acceleration
H	Varying	m	Ice thickness
L	3.34×10^5	$J\ kg^{-1}$	Latent heat of fusion of water
n	3	Dimensionless	Flow law exponent
z_b	Varying	m	Bed elevation with respect to sea level
ν	1.787×10^{-6}	$m^2\ s^{-1}$	Kinematic viscosity of water
ω	0.001	Dimensionless	Parameter controlling nonlinear
			laminar/turbulent transition
ρ_i	917	$kg\ m^{-3}$	Bulk density of ice
ρ_w	1000	$kg\ m^{-3}$	Bulk density of water

Table 2. Velocity observations used for comparison to modeled velocities

File name	Date range	Midpoint date	Reference	Notes
greenland_vel_mosaic500_2000_2001_vv_v02.1.tif	3 September 2000 to 24 January 2001	13 November 2000	Joughin et al. (2015)	--
greenland_vel_mosaic500_2005_2006_vv_v02.1.tif	13 December 2005 to 20 April 2006	15 February 2006	Joughin et al. (2015)	--
greenland_vel_mosaic500_2006_2007_vv_v02.1.tif	18 December 2006 to 6 June 2007	13 March 2007	Joughin et al. (2015)	--
greenland_vel_mosaic500_2007_2008_vv_v02.1.tif	7 September 2007 to 23 April 2008	30 December 2007	Joughin et al. (2015)	--
greenland_vel_mosaic500_2008_2009_vv_v02.1.tif	15 September 2008 to 16 June 2009	30 January 2009	Joughin et al. (2015)	Excluded due to limited data extent.
greenland_vel_mosaic500_2009_2010_vv_v02.1.tif	2 September 2009 to 7 May 2010	30 January 2010	Joughin et al. (2015)	--
greenland_vel_mosaic500_2012_2013_vv_v02.1.tif	10 November 2012 to 5 April 2013	22 January 2013	Joughin et al. (2015)	--
greenland_vel_mosaic500_2014_2015_vv_v02.1.tif	1 September 2014 to 31 May 2015	15 January 2015	Joughin et al. (2015)	--
greenland_vel_mosaic500_2015_2016_vv_v02.1.tif	1 September 2015 to 31 May 2016	15 January 2016	Joughin et al. (2015)	--
greenland_vel_mosaic500_2016_2017_vv_v02.1.tif	1 September 2016 to 31 May 2017	15 January 2017	Joughin et al. (2015)	--
greenland_vel_mosaic500_2017_2018_vv_v02.1.tif	1 September 2017 to 31 May 2018	15 January 2018	Joughin et al. (2015)	--
GL_vel_mosaic_Quarterly_01Dec18_28Feb19_vv_v05.0.tif	1 December 2018 to 28 February 2019	15 January 2019	Joughin et al. (2023)	Regridded to 500m.
GL_vel_mosaic_Quarterly_01Dec19_29Feb20_vv_v05.0.tif	1 December 2019 to 29 February 2020	15 January 2020	Joughin et al. (2023)	Regridded to 500m.

SUPPLEMENTAL FIGURES

S1-S5: Incremental changes between 2004-2008, 2008-2012, 2012-2016, 2016-2020.

S6: Results of experiment exploring the impact on ice velocity due to changes in geometry only, separated from corresponding changes in hydrology.

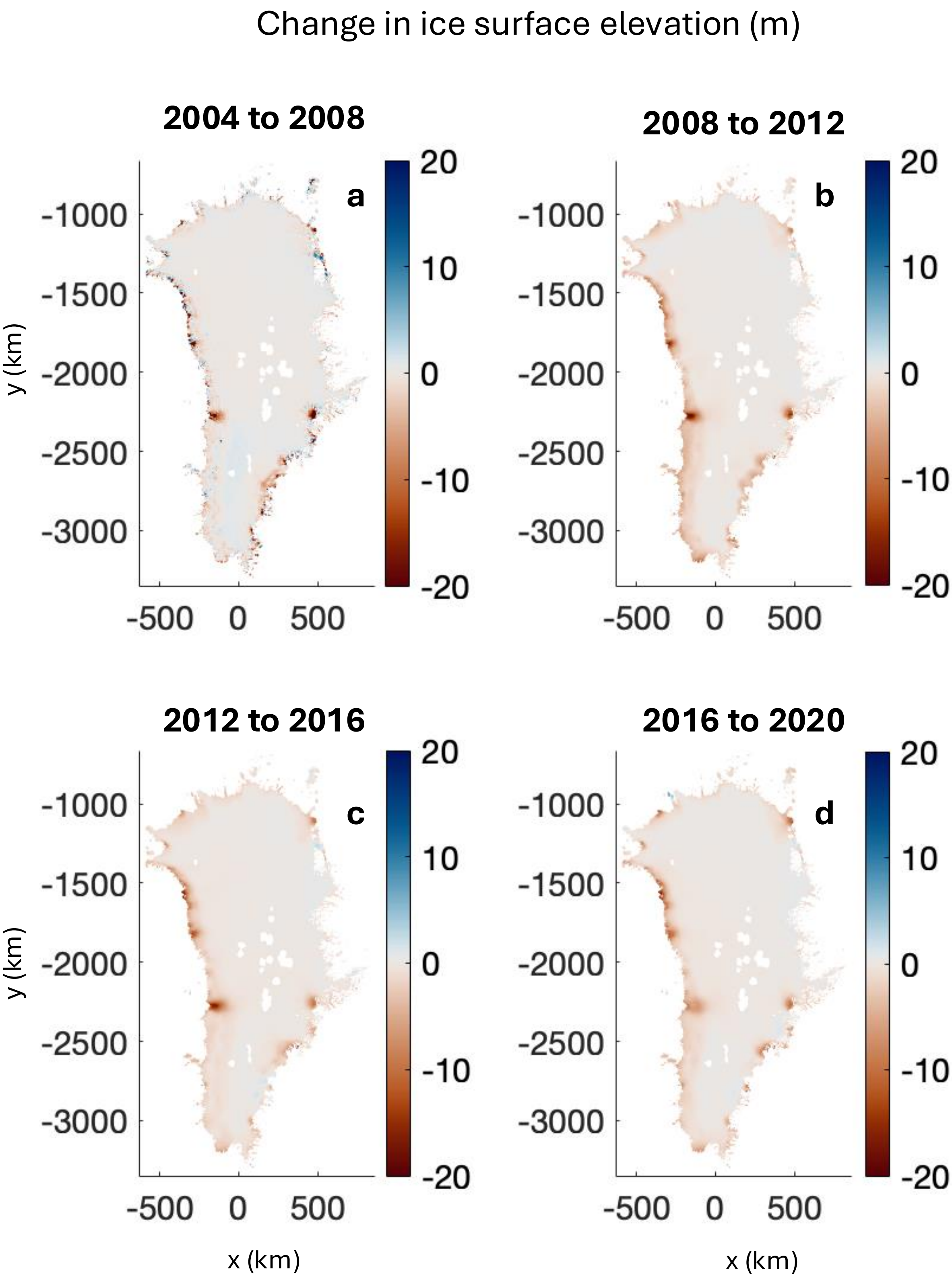

Fig. 1. Change in ice surface elevation of the Greenland Ice Sheet during incremental 4-year periods: a) 2008 minus 2004, b) 2012 minus 2008, c) 2016 minus 2016, d) 2020 minus 2016.

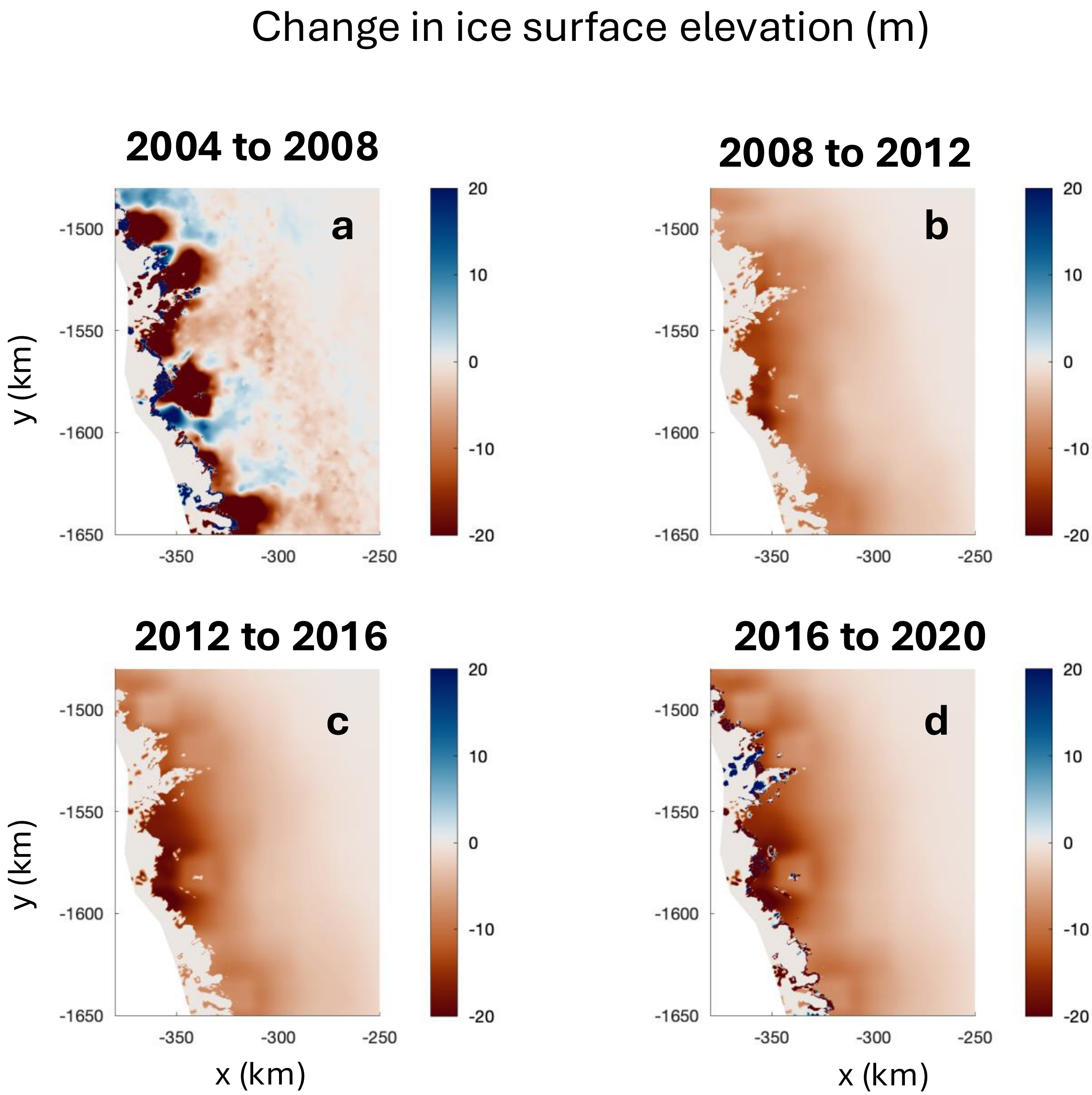

Fig. 2. Change in ice surface elevation in northwest Greenland during incremental 4-year periods: a) 2008 minus 2004, b) 2012 minus 2008, c) 2016 minus 2016, d) 2020 minus 2016.

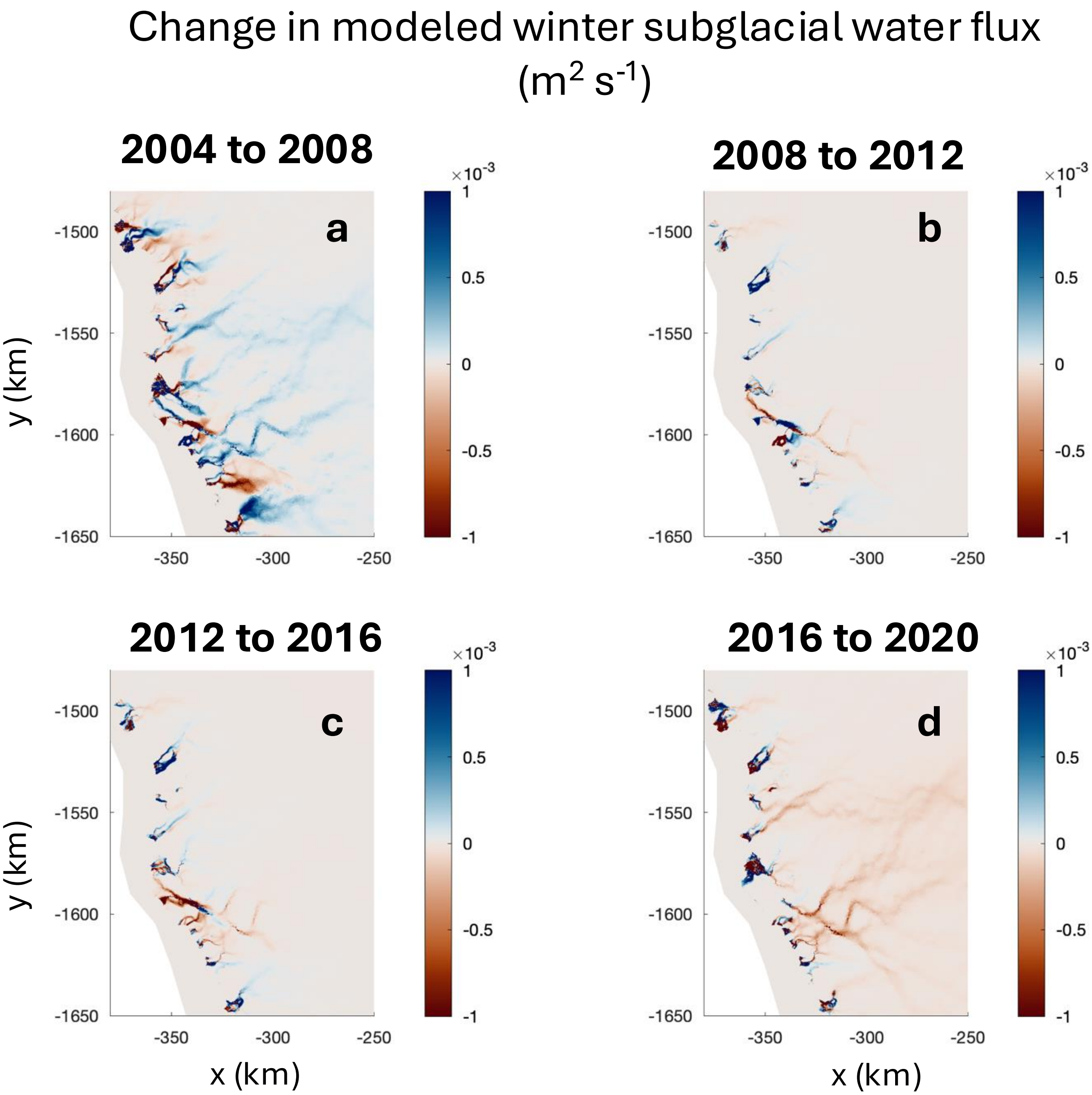

Fig. 3. Change in modeled winter subglacial water flux during incremental 4-year periods: a) 2008 minus 2004, b) 2012 minus 2008, c) 2016 minus 2016, d) 2020 minus 2016.

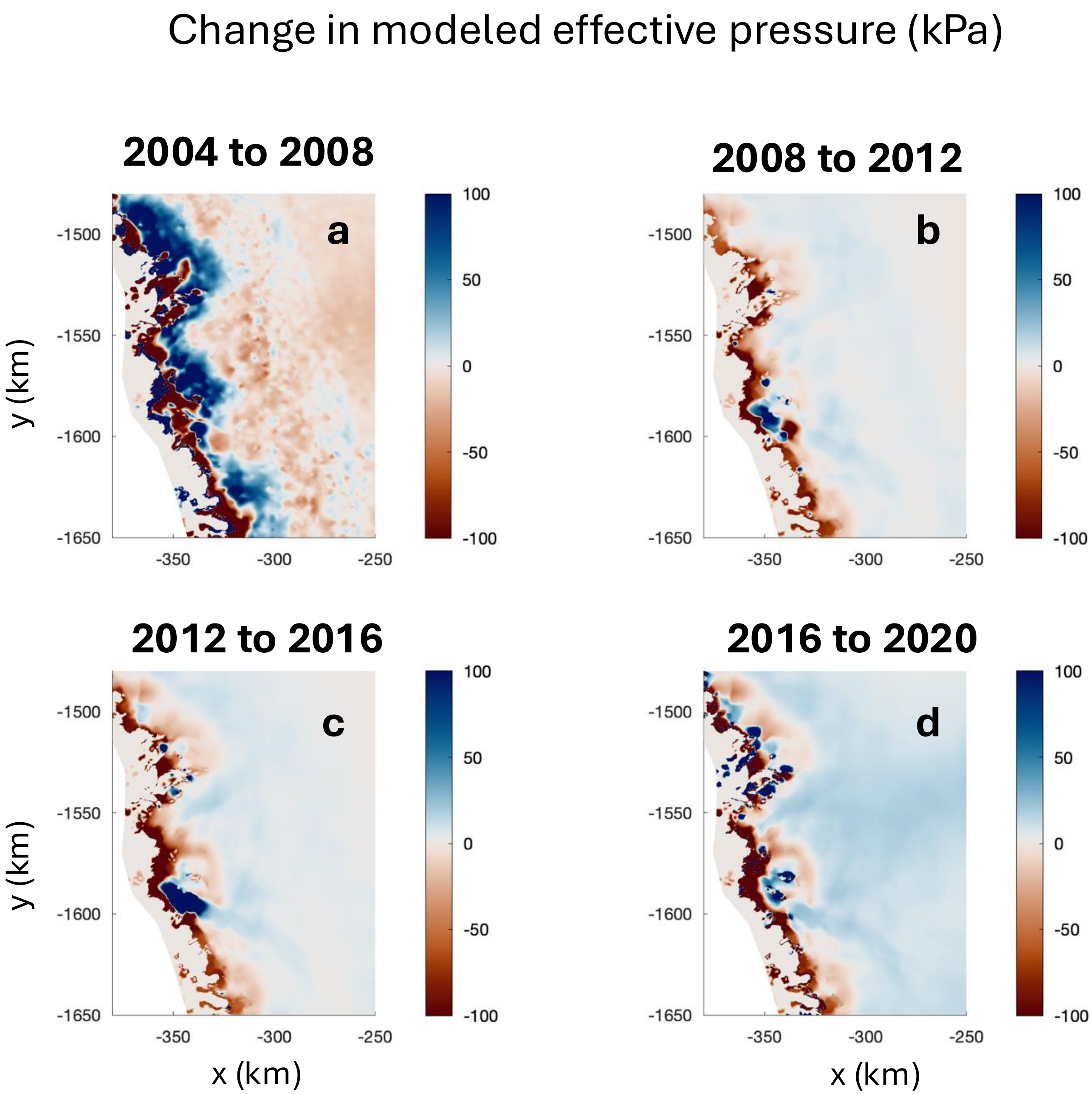

Fig. 4. Change in modeled winter effective pressure during incremental 4-year periods: a) 2008 minus 2004, b) 2012 minus 2008, c) 2016 minus 2016, d) 2020 minus 2016.

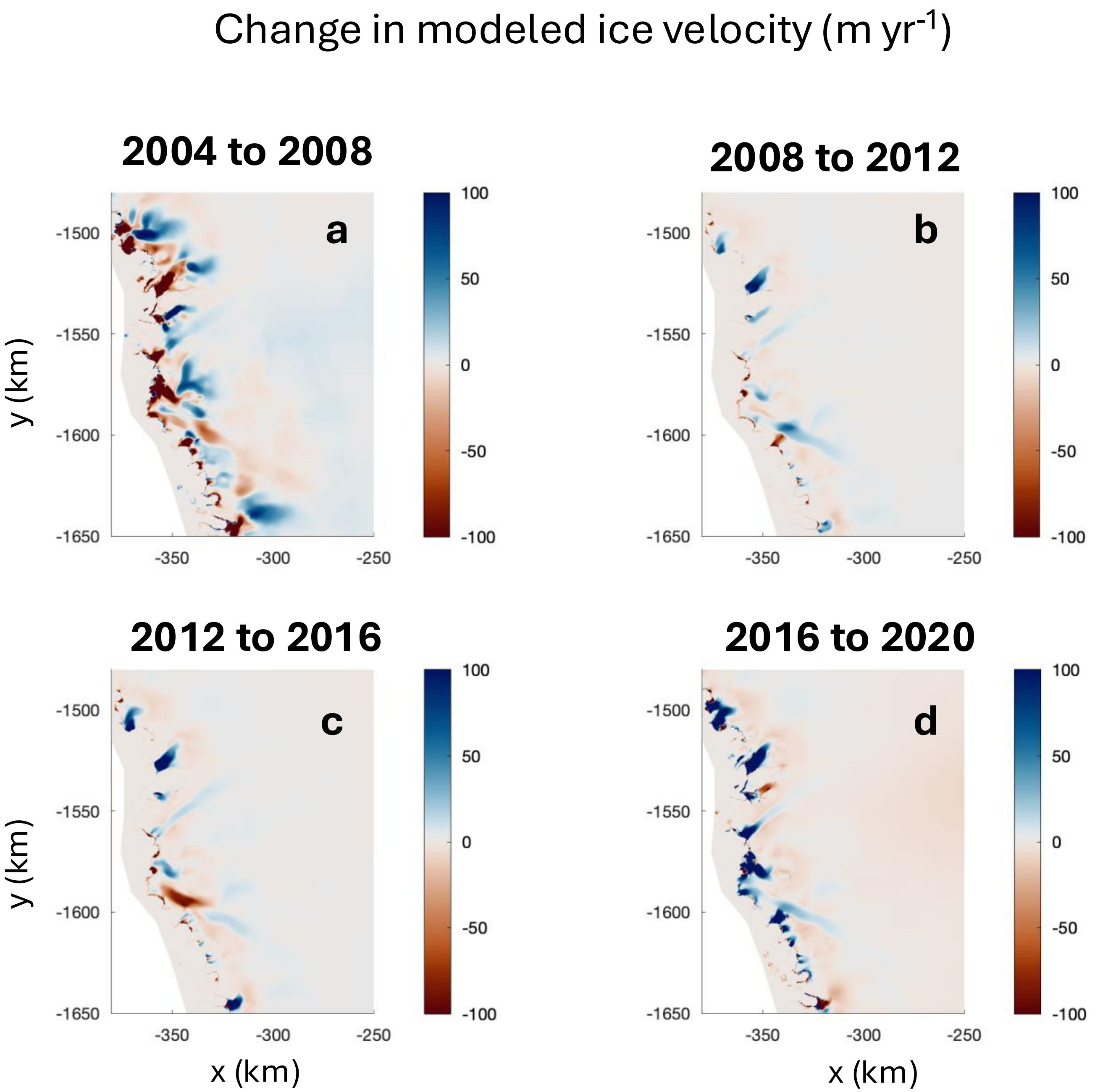

Fig. 5. Change in modeled winter ice velocity during incremental 4-year periods: a) 2008 minus 2004, b) 2012 minus 2008, c) 2016 minus 2016, d) 2020 minus 2016.

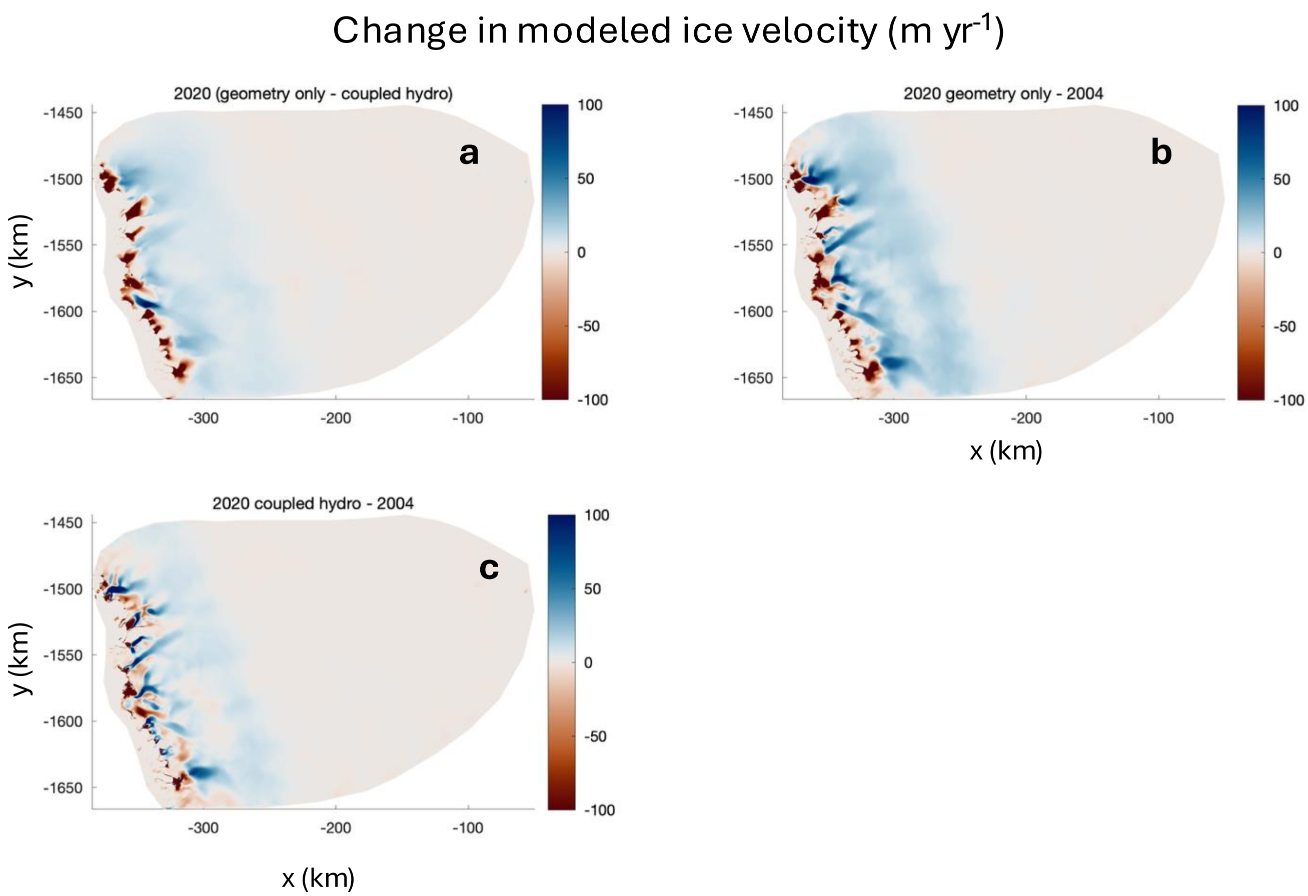

Fig. 6. We conducted an experiment using effective pressure from our 2004 coupled simulation inserted into the 2020 geometry to explore the impact on ice velocity due to changes in geometry only, separated from corresponding changes in hydrology. We refer to this 2020 stress balance with 2004 effective pressure as *N2004*. a) Difference in modeled winter ice velocity with 2020 geometry, between *N2004* and the coupled 2020 simulation. b) Difference in modeled winter ice velocity between *N2004* and the coupled 2004 simulation. c) Difference in modeled winter ice velocity between the 2020 and 2004 coupled simulations (same as shown in Fig. 2d of the main text.

REFERENCES

Blair J and Hofton M (2019) Icebridge lvis l2 geolocated surface elevation product, version 2 (doi: 10.5067/E9E9QSRNLYTK)

Girod L, Nuth C and Kääb A (2015) Improvement of dem generation from aster images using satellite jitter estimation and open source implementation. *The International Archives of the Photogrammetry, Remote Sensing and Spatial Information Sciences*, **XL-1/W5**, 249–253 (doi: 10.5194/isprsarchives-XL-1-W5-249-2015)

Medley B, Neumann T, Zwally H, Smith B and Stevens C (2022) Simulations of firn processes over the Greenland and Antarctic ice sheets: 1980–2021. *The Cryosphere*, **16**(10), 3971–4011 (doi: 10.5194/tc-16-3971-2022)

Porter C, Howat I, Noh M, Husby E, Khuvis S, Danish E, Tomko K, Gardiner J, Negrete A, Yadav B, Klassen J, Kelleher C, Cloutier M, Bakker J, Enos J, Arnold G, Bauer G and Morin P (2022) ArcticDEM – Strips, Version 4.1 (doi: 10.7910/DVN/C98DVS)

Shapiro NM and Ritzwoller MH (2004) Inferring surface heat flux distributions guided by a global seismic model: particular application to Antarctica. *Earth and Planetary Science Letters*, **223**(1-2), 213–224 (doi: 10.1016/j.epsl.2004.06.024)

Shean DE, Alexandrov O, Moratto ZM, Smith BE, Joughin IR, Porter C and Morin P (2016) An automated, open-source pipeline for mass production of digital elevation models (dems) from very-high-resolution commercial stereo satellite imagery. *ISPRS Journal of Photogrammetry and Remote Sensing*, **116**, 101–117

Shean DE, Joughin IR, Dutrieux P, Smith BE and Berthier E (2019) Ice shelf basal melt rates from a high-resolution digital elevation model (dem) record for pine island glacier, antarctica. *The Cryosphere*, **13**(10), 2633–2656 (doi: 10.5194/tc-13-2633-2019)

Smith B, Fricker HA, Holschuh N, Gardner AS, Adusumilli S, Brunt KM, Csatho B, Harbeck K, Huth A, Neumann T and others (2019) Land ice height-retrieval algorithm for NASA's ICESat-2 photon-counting laser altimeter. *Remote Sensing of Environment*, **233**, 111352 (doi: 10.1016/j.rse.2019.111352)

Smith B, Dickinson S, Jelley B, Neumann T, Hancock D, Lee J and Harbeck K (2025a) Atlas/icesat-2 l3b slope-corrected land ice height time series, version 7 (doi: 10.5067/ATLAS/ATL11.007)

Smith B, Jelley BP, Dickinson S, Sutterley T, Neumann T and Harbeck K (2025b) Atlas/icesat-2 l3b gridded antarctic and greenland height change, version 5 (doi: 10.5067/ATLAS/ATL15.005)

Smith B, Sutterley TC, Fricker HA, Padman L, Siegfried MR, Black T, Felikson D, Freer BID, Gibbons A, Howard SL and et al (2026) Icesat-2 land ice products resolve greenland and antarctic ice-sheet height changes on seasonal to multiyear time scales. *Journal of Glaciology*, 1–55 (doi: 10.1017/jog.2026.10152)

Studinger M (2014) Icebridge atm l2 icessn elevation, slope, and roughness, version 2 (doi: 10.5067/CPRXXK3F39RV)

Zwally H, Schutz R, Dimarzio J and Hancock D (2014) Glas/icesat l1b global elevation data (hdf5), version 34 (doi: 10.5067/ICESAT/GLAS/DATA109)